Article

Cell

A Heterochromatin-Specific RNA Export Pathway Facilitates piRNA Production

Graphical Abstract

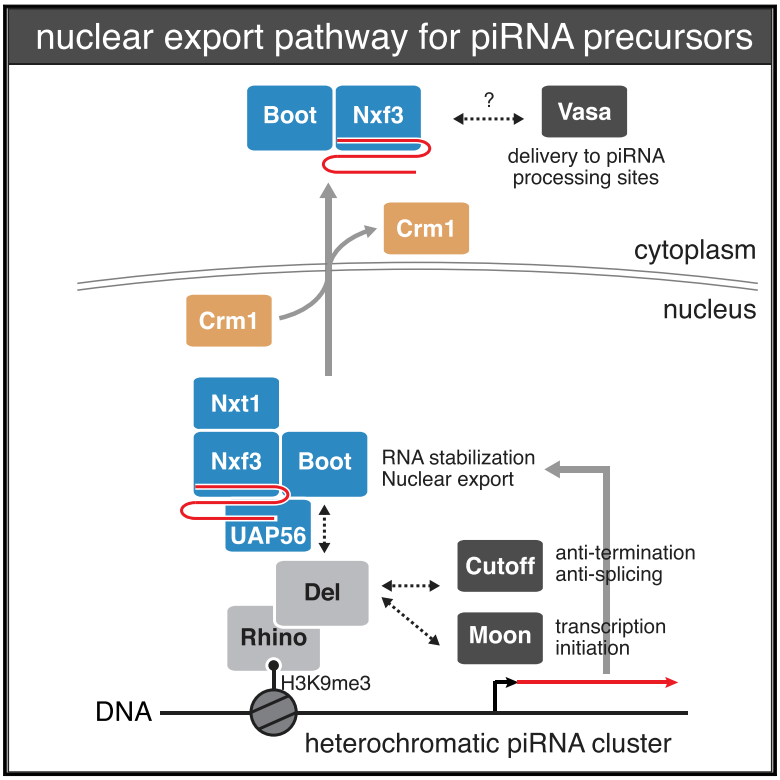

Highlights

- The Nxf3 pathway: nuclear export for heterochromatic piRNA precursors in *Drosophila*
- Nxf3 obtains chromatin-mediated RNA cargo specificity through the Bootlegger protein
- The Nxf3 pathway mediates retrovirus-like evasion of nuclear RNA surveillance
- Nxf3-Bootlegger deliver piRNA precursors to cytoplasmic processing granules

Authors

Mostafa F. ElMaghraby, Peter Refsing Andersen, Florian Pühringer, ..., Thomas Lendl, Laszlo Tirian, Julius Brennecke

Correspondence

pra@mbg.au.dk (P.R.A.), julius.brennecke@imba.oeaw.ac.at (J.B.)

In Brief

Heterochromatic piRNA precursors escape classic mRNA quality-control and surveillance mechanisms through a dedicated nuclear export pathway.

ElMaghraby et al., 2019, Cell *178*, 964–979
August 8, 2019
https://doi.org/10.1016/j.cell.2019.07.007

CellPress

Cell

Article

A Heterochromatin-Specific RNA Export Pathway Facilitates piRNA Production

Mostafa F. ElMaghraby,[1,4] Peter Refsing Andersen,[1,3,4,*] Florian Pühringer,[1] Ulrich Hohmann,[1,2] Katharina Meixner,[1] Thomas Lendl,[1,2] Laszlo Tirian,[1] and Julius Brennecke[1,5,*]

[1]Institute of Molecular Biotechnology of the Austrian Academy of Sciences (IMBA), Vienna BioCenter (VBC), Dr. Bohrgasse 3, 1030 Vienna, Austria

[2]Institute of Molecular Pathology (IMP), Vienna BioCenter (VBC), Campus-Vienna-Biocenter 1, 1030 Vienna, Austria

[3]Present address: Department of Molecular Biology and Genetics, Aarhus University, C. F. Møllers Allé 3, 8000 Aarhus, Denmark

[4]These authors contributed equally

[5]Lead Contact

*Correspondence: pra@mbg.au.dk (P.R.A.), julius.brennecke@imba.oeaw.ac.at (J.B.)

https://doi.org/10.1016/j.cell.2019.07.007

SUMMARY

PIWI-interacting RNAs (piRNAs) guide transposon silencing in animals. The 22–30 nt piRNAs are processed in the cytoplasm from long non-coding RNAs that often lack RNA processing hallmarks of export-competent transcripts. By studying how these transcripts achieve nuclear export, we uncover an RNA export pathway specific for piRNA precursors in the *Drosophila* germline. This pathway requires Nxf3-Nxt1, a variant of the hetero-dimeric mRNA export receptor Nxf1-Nxt1. Nxf3 interacts with UAP56, a nuclear RNA helicase essential for mRNA export, and CG13741/Bootlegger, which recruits Nxf3-Nxt1 and UAP56 to heterochromatic piRNA source loci. Upon RNA cargo binding, Nxf3 achieves nuclear export via the exportin Crm1 and accumulates together with Bootlegger in peri-nuclear nuage, suggesting that after export, Nxf3-Bootlegger delivers precursor transcripts to the piRNA processing sites. These findings indicate that the piRNA pathway bypasses nuclear RNA surveillance systems to export unprocessed transcripts to the cytoplasm, a strategy also exploited by retroviruses.

INTRODUCTION

Integrity of the germline genome is essential for the survival of multicellular species. In animal gonads, a class of small regulatory RNAs, called PIWI-interacting RNAs (piRNAs), guide Argonaute effector proteins to silence transposable elements, thereby counteracting their mutagenic impact (Czech et al., 2018; Ozata et al., 2018; Siomi et al., 2011). piRNAs are processed from single-stranded precursors, which are transcribed by RNA polymerase II from transposon-rich loci termed piRNA clusters. As piRNA biogenesis occurs in peri-nuclear processing centers, the long non-coding precursor transcripts must be exported from the nucleus to the cytoplasm.

mRNAs, the most prominent RNA polymerase II transcripts, are exported through nuclear pore complexes primarily by the nuclear RNA export factor 1 (Nxf1/Tap) and its binding partner Nxt1/p15 (Cullen, 2000; Köhler and Hurt, 2007; Reed and Hurt, 2002). The Nxf1-Nxt1 heterodimer is recruited to export-competent mRNAs after successful completion of RNA-processing events such as 5′ capping, splicing, and 3′ end formation (Heath et al., 2016). Nuclear mRNA surveillance systems ensure that unprocessed transcripts are not exported but instead are degraded within the nucleus. mRNA processing is therefore a critical step in licensing export of RNA polymerase II transcripts to the cytoplasm.

In *Drosophila*, only few piRNA precursors are spliced and polyadenylated, and these require the mRNA export receptor Nxf1-Nxt1 for nuclear exit (Dennis et al., 2016; Goriaux et al., 2014; Mohn et al., 2014). Most piRNA precursors instead lack RNA processing marks characteristic for mRNAs. These precursors originate from heterochromatic loci, whose expression depends on Rhino, a variant of the conserved heterochromatin protein 1 (HP1) (Klattenhoff et al., 2009). Rhino, via its adaptor protein Deadlock, recruits effector proteins that stimulate transcription initiation within heterochromatin (through the TFIIA-L homolog Moonshiner) (Andersen et al., 2017), and that suppress co-transcriptional RNA processing events such as splicing or 3′ cleavage and polyadenylation (through the Rai1 homolog Cutoff) (Chen et al., 2016; Mohn et al., 2014; Zhang et al., 2014). Rather than imposing transcriptional silencing similar to HP1, Rhino thereby facilitates non-canonical transcription of heterochromatic piRNA source loci to allow the production of non-coding precursors for transposon-targeting piRNAs. How the resulting unprocessed piRNA precursors escape nuclear RNA quality control and how they are transported to cytoplasmic piRNA processing centers are central open questions.

Here, we identify a nuclear export pathway dedicated to piRNA precursors. It involves Nuclear export factor 3 (Nxf3), which is required for piRNA production, transposon silencing, and fertility and which evolved from the principal mRNA-export receptor Nxf1. Instead of relying on RNA processing events for recruitment, Nxf3 is targeted to nascent piRNA precursors via Rhino, Deadlock, and CG13741/Bootlegger, a previously unknown effector protein of Rhino-dependent heterochromatin

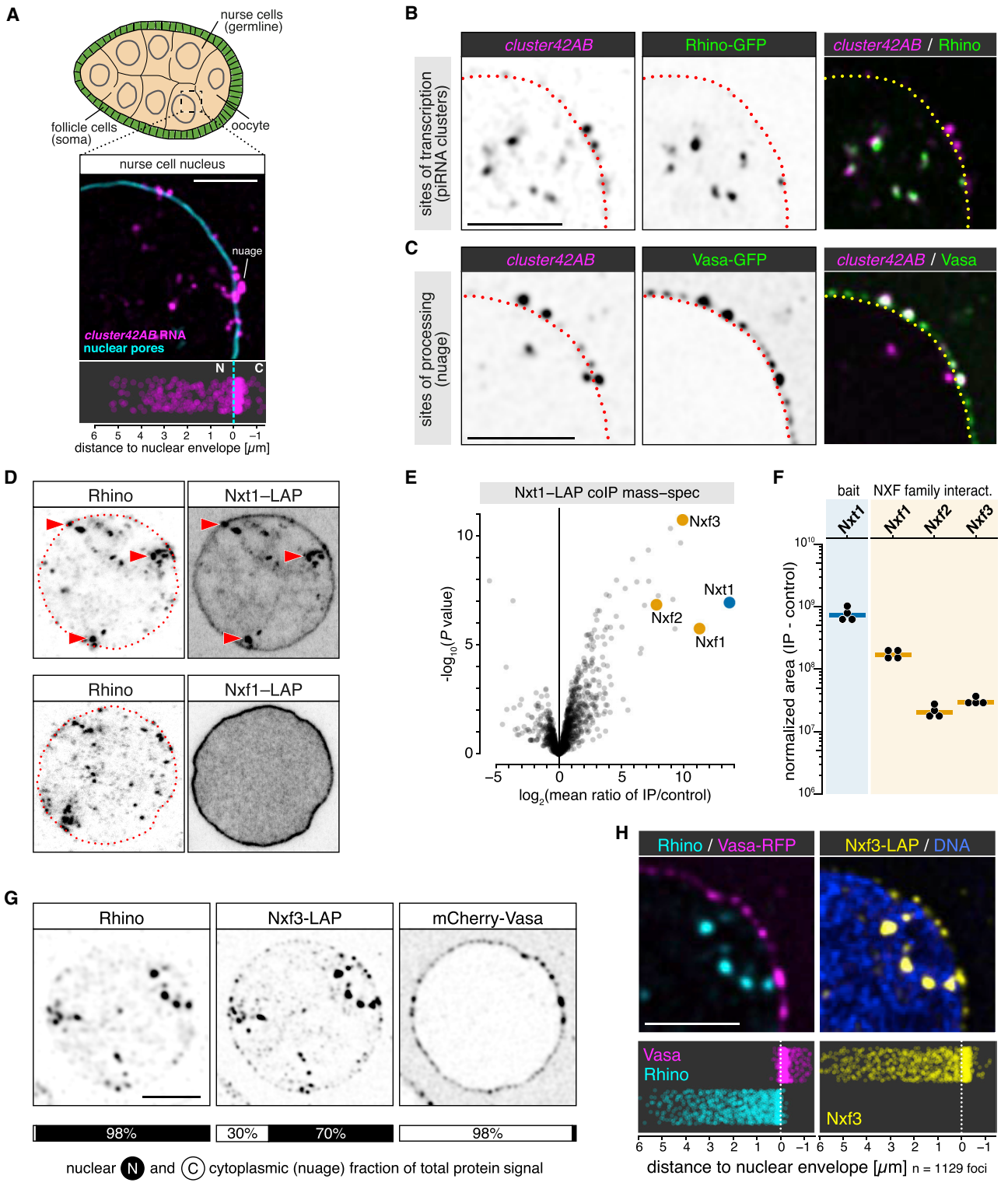

Figure 1. Nxf3 Localizes to piRNA Clusters and Nuage

(A) Top: *Drosophila* stage 7 egg chamber (nurse cells: germline, beige; somatic cells: green). Middle: confocal image (scale bar: 5 μm) showing part of a nurse cell nucleus; nuclear pores stained with wheat germ agglutinin (cyan); piRNA *cluster42AB* precursor in magenta (RNA FISH). Bottom: positions of *cluster42AB* RNA FISH foci relative to nuclear envelope (n = 509 from 11 nuclei).

(legend continued on next page)

expression. After cargo binding, Nxf3 mediates piRNA precursor export in a Crm1/Xpo1-dependent manner, allowing Nxf3 and Bootlegger to deliver piRNA precursors to peri-nuclear nuage where piRNA biogenesis factors accumulate. This dedicated RNA export pathway—formed by Nxf1 duplication and neo-functionalization—therefore bypasses nuclear RNA surveillance systems and transports piRNA precursors from their heterochromatic origins to their cytoplasmic processing sites.

RESULTS

Nxf3 Localizes to piRNA Transcription and Processing Sites

To visualize the transport route of Rhino-dependent piRNA precursors in ovaries, we performed fluorescent *in situ* hybridization (RNA FISH) experiments directed against transcripts from piRNA *cluster42AB*, the most prominent piRNA source locus genome-wide (Brennecke et al., 2007). *cluster42AB* transcripts were enriched in nuclear foci as well as in cytoplasmic foci lining the nuclear envelope (Figure 1A; Figure S1A). The nuclear foci correspond to piRNA clusters where Rhino licenses piRNA precursor transcription (Figure 1B) (Klattenhoff et al., 2009; Mohn et al., 2014; Zhang et al., 2014). The peri-nuclear foci in the cytoplasm mark "nuage," electron-dense RNP granules where Vasa and other factors orchestrate piRNA biogenesis (Figure 1C) (Lim and Kai, 2007; Mahowald, 1971; Malone et al., 2009; Zhang et al., 2012).

Export of mRNA from the nucleus requires the association of the heterodimeric nuclear RNA export receptor Nxf1-Nxt1 (Tap-p15) with mRNA cargo, which is enabled by the nuclear RNA helicase UAP56/Hel25E and the associated THO complex, present from yeast to human (Heath et al., 2016; Köhler and Hurt, 2007; Luo et al., 2001; Strässer and Hurt, 2001). In the *Drosophila* germline, both UAP56 and the THO complex are enriched at Rhino-dependent piRNA clusters and are required for efficient piRNA production from these loci (Hur et al., 2016; Zhang et al., 2012, 2018). To ask whether Nxf1-Nxt1 might also export germline piRNA precursors, we generated flies expressing Nxf1 or Nxt1 with a "localization and affinity purification" (LAP) tag consisting of GFP and a triple FLAG peptide. Nxt1-LAP was enriched at nuclear Rhino foci (Figure 1D). Nxf1-LAP instead was uniformly distributed in the nucleus, with enrichment at the nuclear envelope, as also seen for Nxt1-LAP (Figure 1D). This suggested that the mRNA export co-factor Nxt1 functions at Rhino-dependent piRNA clusters, probably in a Nxf1-independent manner.

To identify proteins acting together with Nxt1 at piRNA clusters, we affinity-purified Nxt1-LAP from ovary lysates and analyzed co-eluting proteins by quantitative mass spectrometry. In addition to Nxf1, the NXF variants Nxf2 and Nxf3 were highly enriched in Nxt1-LAP eluates (Figure 1E), albeit with lower peptide levels (Figure 1F). We confirmed these findings using an independent fly line, expressing HA-tdTomato-tagged Nxt1 from the endogenous locus (Figures S1B and S1C). Nxf2 and Nxf3 are expressed predominantly in ovaries (Figure S1D) (Brown et al., 2014) and were genetically identified as putative piRNA pathway factors (Czech et al., 2013). As Nxf2 acts in piRNA-guided heterochromatin formation, and not in nuclear mRNA or piRNA precursor export (Batki et al., 2019; Fabry et al., 2019; Murano et al., 2019; Zhao et al., 2019), we focused on Nxf3, an orphan NXF variant with unknown function (Herold et al., 2000, 2001, 2003).

Tagging the endogenous *nxf3* locus with a C-terminal LAP-tag revealed Nxf3 expression specifically in nurse cells (Figure S1E). Its nuclear localization strongly overlapped with that of Rhino (Figures 1G and 1H), indicating that Nxf3 functions at piRNA clusters together with Nxt1. However, unlike the strictly nuclear Rhino protein, Nxf3-LAP was also enriched in cytoplasmic foci lining the nuclear envelope (Figures 1G and 1H). All of these cytoplasmic Nxf3 foci were positive for the piRNA biogenesis factor Vasa, indicating that they represent nuage granules. Indeed, immuno-gold electron microscopy revealed localization of Nxf3-LAP within peri-nuclear, electron-dense nuage compartments, as well as in adjacent nuclear regions (Figures S1F and S1G) where Rhino is often observed (Zhang et al., 2012).

Of all known proteins localizing to Rhino-dependent piRNA clusters, Nxf3 is unique in that it is also enriched in nuage. Considering this dual localization, together with Nxf3's homology to the mRNA export receptor Nxf1 (Herold et al., 2000), we hypothesized that Nxf3 is recruited to Rhino-dependent piRNA clusters from where it transports piRNA precursors through nuclear pore complexes (NPCs) to cytoplasmic piRNA processing centers.

piRNA Precursor Export Requires Nxf3

Our model predicts that Nxf3 is required for efficient mature piRNA production. To test this, we generated flies carrying *nxf3*-null alleles (Figures S2A and S2B). Based on small RNA sequencing, ovaries lacking Nxf3 exhibited ~5- to 10-fold reduced levels of piRNAs originating from Rhino-dependent piRNA source loci (Figures 2A–2C). In contrast, piRNAs originating from the Rhino-independent piRNA source loci *cluster20A* or *flamenco* (Klattenhoff et al., 2009; Mohn et al., 2014) were not reduced in *nxf3* mutant ovaries (Figures 2B and 2C). In line with this, Rhino-independent piRNA precursors are spliced, poly-adenylated and exported by Nxf1-Nxt1 (Dennis et al., 2016; Goriaux et al., 2014; Mohn et al., 2014).

(B and C) Confocal images (scale bars: 5 μm) showing *cluster42AB* transcripts and GFP-Rhino (B) or GFP-Vasa (C) in nurse cells (dotted line: nuclear envelope; see Figure S1A).
(D) Localization of Nxt1-LAP or Nxf1-LAP (right) alongside Rhino (left) in nurse cells (dotted line: nuclear envelope).
(E) Enrichment values and corresponding significance levels for proteins co-purifying with Nxt1-LAP versus control (nuclear LAP) from ovary lysates (n = 3).
(F) Peptide peak intensities (experiment minus respective replicate control) for the Nxt1-LAP bait and the protein interactors marked in (E) (bars: median values).
(G) Inverted confocal image of a nurse cell nucleus (scale bar: 5 μm) showing localization of Rhino, mCherry-Vasa, and Nxf3-LAP. Cartoons indicate sum of nuclear and cytoplasmic signal intensities of >1,000 foci per protein.
(H) Part of nucleus (scale bar: 5 μm) shown in (G) indicating localization of Nxf3-LAP (yellow), Rhino (cyan), and mCherry-Vasa (magenta). Jitter plots show positions of indicated protein foci relative to nuclear envelope (>1,000 foci per protein).
See also Figure S1.

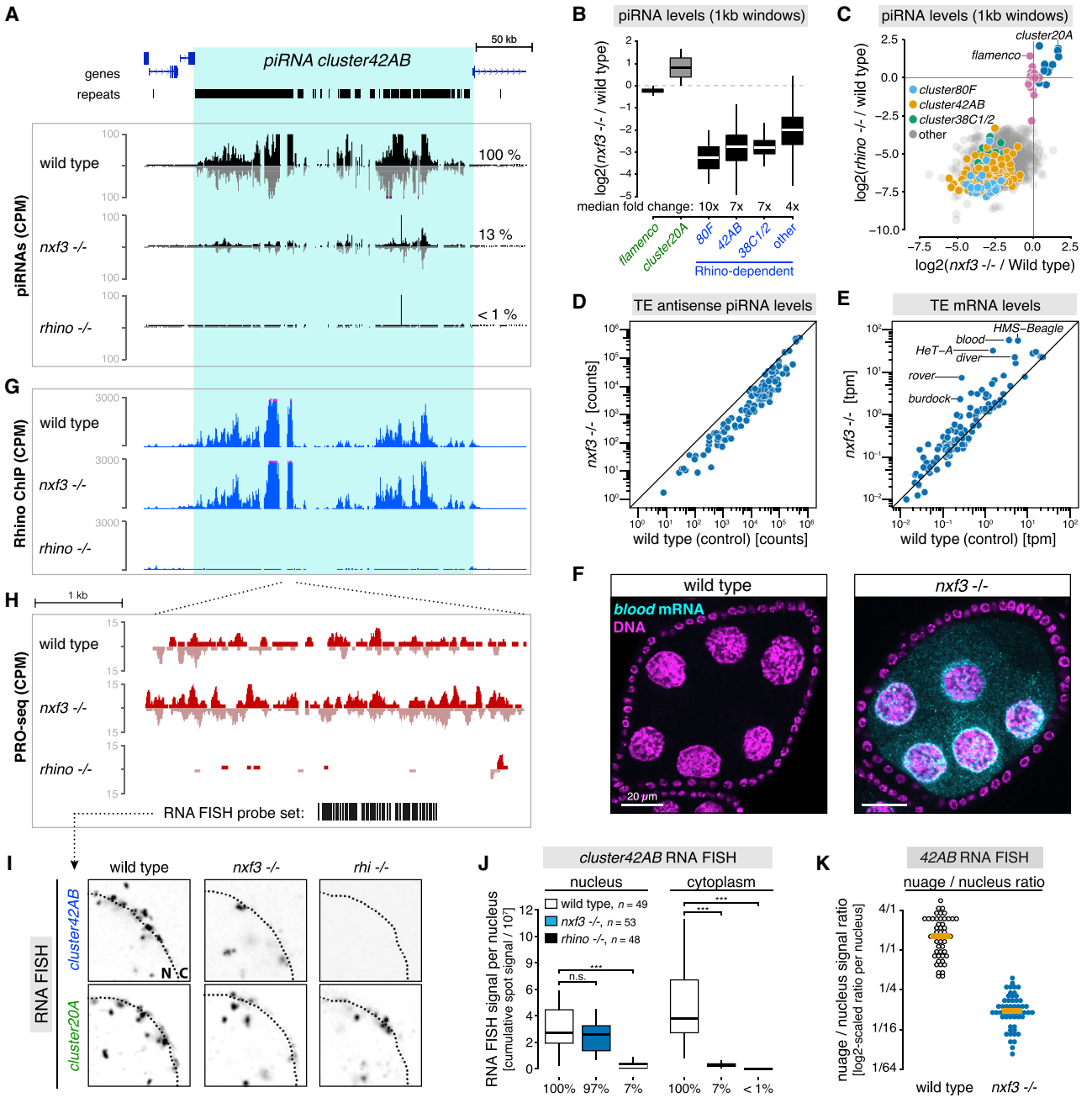

Figure 2. Nxf3 Is Required for piRNA Precursor Export

(A) UCSC genome browser panel showing ovarian piRNA levels (CPM, coverage per million miRNA reads) at *cluster42AB* in indicated genotypes.

(B) Changes in piRNA levels for indicated clusters (split into 1-kb tiles) in *nxf3* mutants, relative to control (*w[1118]*). Boxplot displays median (line), first and third quartiles (box), and highest or lowest value within 1.5× interquartile range (whiskers).

(C) log2 fold changes of piRNAs mapping uniquely to 1-kb tiles from Rhino-dependent piRNA clusters in *rhino* versus *nxf3* mutants (relative to control). Tiles from major piRNA clusters are colored; *cluster20A* and *flamenco* tiles serve as Rhino-independent control group.

(D and E) Levels of antisense piRNAs (D) or sense mRNA reads (E) mapping to consensus transposon sequences from control versus *nxf3* mutant ovary samples.

(F) Confocal images of wild-type (left) and *nxf3* mutant (right) egg chambers showing *blood* transposon mRNA (FISH: cyan; DAPI stain: magenta).

(G) UCSC genome browser panel showing Rhino occupancy (chromatin immuno-precipitation sequencing [ChIP-seq]; CPM, coverage per million reads) at *cluster42AB* in indicated genotypes.

(H) 5-kb part of *cluster42AB* with PRO-seq signal from indicated genotypes in red. Black bars indicate 48 oligo FISH probes used in (I)–(K).

(I) Representative confocal images of parts of germline nuclei (genotypes indicated) stained with RNA-FISH for *cluster42AB* transcripts (Rhino-dependent) and *cluster20A* transcripts (Rhino-independent).

(legend continued on next page)

For many germline-active transposons, the loss of piRNAs from Rhino-dependent source loci resulted in ~10-fold reduced levels of antisense, silencing-competent piRNAs (Figure 2D; Figures S2C and S2D). Consistent with this, several transposons were de-repressed in *nxf3* mutant ovaries (Figure 2E; Figure S2E). Among them are *blood* (Figure 2F; Figure S2F), *HMS-Beagle*, *rover*, *diver*, and *HeT-A*, retro-transposons whose de-silencing has been linked to severe oocyte DNA damage in piRNA pathway mutants (Durdevic et al., 2018; Senti et al., 2015; Wang et al., 2018). Indeed, *nxf3* mutants were female sterile, despite globally unperturbed levels of ovarian mRNAs (Figures S2G and S2H).

To determine how Nxf3 loss impairs piRNA production, we analyzed whether Rhino-dependent piRNA source loci are still specified and transcribed in *nxf3* mutants. Rhino's genome-wide enrichment at piRNA clusters was unchanged in *nxf3* mutant ovaries (Figure 2G; Figure S2I), as was the localization of factors co-localizing with Rhino at piRNA clusters (e.g., Deadlock, Cutoff, Moonshiner, UAP56; Figures S3A–S3D) (Andersen et al., 2017; Mohn et al., 2014; Pane et al., 2011; Wehr et al., 2006; Zhang et al., 2012, 2014). piRNA cluster transcription, as determined by global precision nuclear run-on sequencing (PRO-seq) (Kwak et al., 2013), was also virtually unchanged in *nxf3* mutant ovaries (Figure 2H; Figure S2I). The observed piRNA losses in *nxf3* mutants must therefore be due to defects downstream of piRNA cluster specification and transcription.

To assay the fate of piRNA precursors in *nxf3* mutants, we determined the subcellular localization of *cluster42AB* and *cluster80F* transcripts, with the Rhino-independent *cluster20A* serving as a control. In *rhino* mutants, nuclear and cytoplasmic foci (marking transcription and piRNA biogenesis sites, respectively) from *cluster42AB* and *cluster80F* were lost (Figures 2I and 2J; Figure S2J). The nuclear *cluster42AB* and *cluster80F* foci were unaffected in *nxf3* mutants (Figures 2I and 2J; Figure S2J), consistent with the PRO-seq data (Figure 2H), whereas loss of Nxf3 substantially reduced the cytoplasmic *cluster42AB* and *cluster80F* signals (Figures 2I–2K; Figure S2J). By contrast, nuclear and cytoplasmic accumulation of Rhino-independent *cluster20A* transcripts was unaffected in *nxf3* mutants (Figure 2I; Figures S3E and S3F). As transcripts from *cluster42AB* or *cluster80F* did not accumulate in *nxf3* mutant nurse cell nuclei, our findings indicate that piRNA precursors, which cannot be exported in the absence of Nxf3, are instead targeted for degradation in the nucleus. Consistent with this, we observed an ~2- to 3-fold reduction in steady-state RNA levels from Rhino-dependent piRNA clusters (Figures S3G and S3H). Altogether, our data support a direct role for Nxf3 in stabilization and nuclear export of Rhino-dependent piRNA cluster transcripts. We note that piRNA loss and transposon de-repression were less severe in *nxf3* mutants compared to *rhino* mutants, potentially indicating low-level nuclear export of piRNA precursors by the canonical mRNA export receptor Nxf1-Nxt1.

Nxf3 Binds piRNA Precursors

Nxf3-LAP extensively co-localized with *cluster42AB* transcripts in the nucleus and nuage (Figure 3A). Supporting a direct interaction between Nxf3 and RNA, electrophoretic mobility shift assays revealed that Nxf3's N-terminal RRM-LRR domain (RNA recognition motif and Leucine-rich repeat) is capable of RNA binding *in vitro* (Figures S4A and S4B). To test whether Nxf3 associates with Rhino-dependent piRNA precursors *in vivo*, we performed RNA immuno-precipitation (RIP) experiments on Nxf3-LAP-expressing ovaries, ovaries expressing UAP56-LAP (which binds Rhino-dependent piRNA precursors) (Zhang et al., 2012, 2018), and ovaries expressing nuclear LAP alone. Based on qRT-PCR, Nxf3-LAP RIP eluates recovered ~10% of *cluster42AB* transcripts present in the lysate (input) (Figure 3B). This recovery was in a similar range compared to UAP56-LAP RIP and several 100-fold more than in the LAP control eluate. In contrast, transcripts from the Rhino-independent piRNA *cluster20A*, abundant house-keeping mRNAs, or rRNAs were not enriched above background in Nxf3-LAP RIP eluates (Figure 3B).

To identify Nxf3 cargo genome-wide, we sequenced libraries generated from the RIP eluates. Transcripts from all major Rhino-dependent piRNA source loci, but not those from Rhino-independent source loci (e.g., *cluster20A*) or mRNAs, were enriched several 100-fold above background in Nxf3-LAP eluates (Figure 3C). The RNA helicase UAP56 also associated with Rhino-dependent piRNA precursors (Figure 3D) (Zhang et al., 2012, 2018). Unlike Nxf3, however, UAP56 bound also mRNAs, consistent with its role in mRNA export upstream of Nxf1-Nxt1 (Köhler and Hurt, 2007). While most mRNAs were enriched in the UAP56-RIP libraries, this varied from no measurable enrichment (often for highly abundant transcripts like ribosomal protein-encoding mRNAs) to up to 50-fold enrichment (e.g., transcription factor encoding genes like *vrille* or *schnurri*; Figure S4C), probably reflecting the ratio of nuclear versus cytoplasmic transcripts for the different mRNAs.

Besides the few major germline piRNA clusters, Rhino is also enriched at hundreds of other genomic loci, mainly located in peri-centromeric heterochromatin (Mohn et al., 2014; Zhang et al., 2014). The RIP libraries revealed that, genome-wide, Rhino-bound loci (a total of 2,996 genomic 1-kb tiles; RD-SL tiles in Figure 3E) give rise to transcripts that associate with both Nxf3 and UAP56 (Figure 3E; Figures S4D and S4E). In contrast, transcripts from tiles overlapping expressed gene loci (~25,000 1-kb tiles; not bound by Rhino) were bound by UAP56, but not by Nxf3 (Figure 3E; Figures S4D and S4E). Our data indicate that, in addition to its role in generating mRNP complexes competent for Nxf1-Nxt1-mediated export, UAP56 may play an analogous function at piRNA clusters in connection with Nxf3-Nxt1.

Inspection of Nxf3-bound transcripts originating from distinct piRNA clusters revealed that top and bottom strand precursors were asymmetrically distributed relative to Rhino's chromatin occupancy. For example, the first third of *cluster80F* was

(J) Quantification of *cluster42AB* RNA FISH signal in nurse cells with indicated genotype (boxplot definition as in (B); ***$p < 0.0001$ based on Mann-Whitney-Wilcoxon test; n: number of analyzed nuclei per genotype).
(K) Ratio of total *cluster42AB* RNA FISH signal in nuage versus nucleus quantified per nucleus (genotypes indicated; orange bars: median values).
See also Figures S2 and S3.

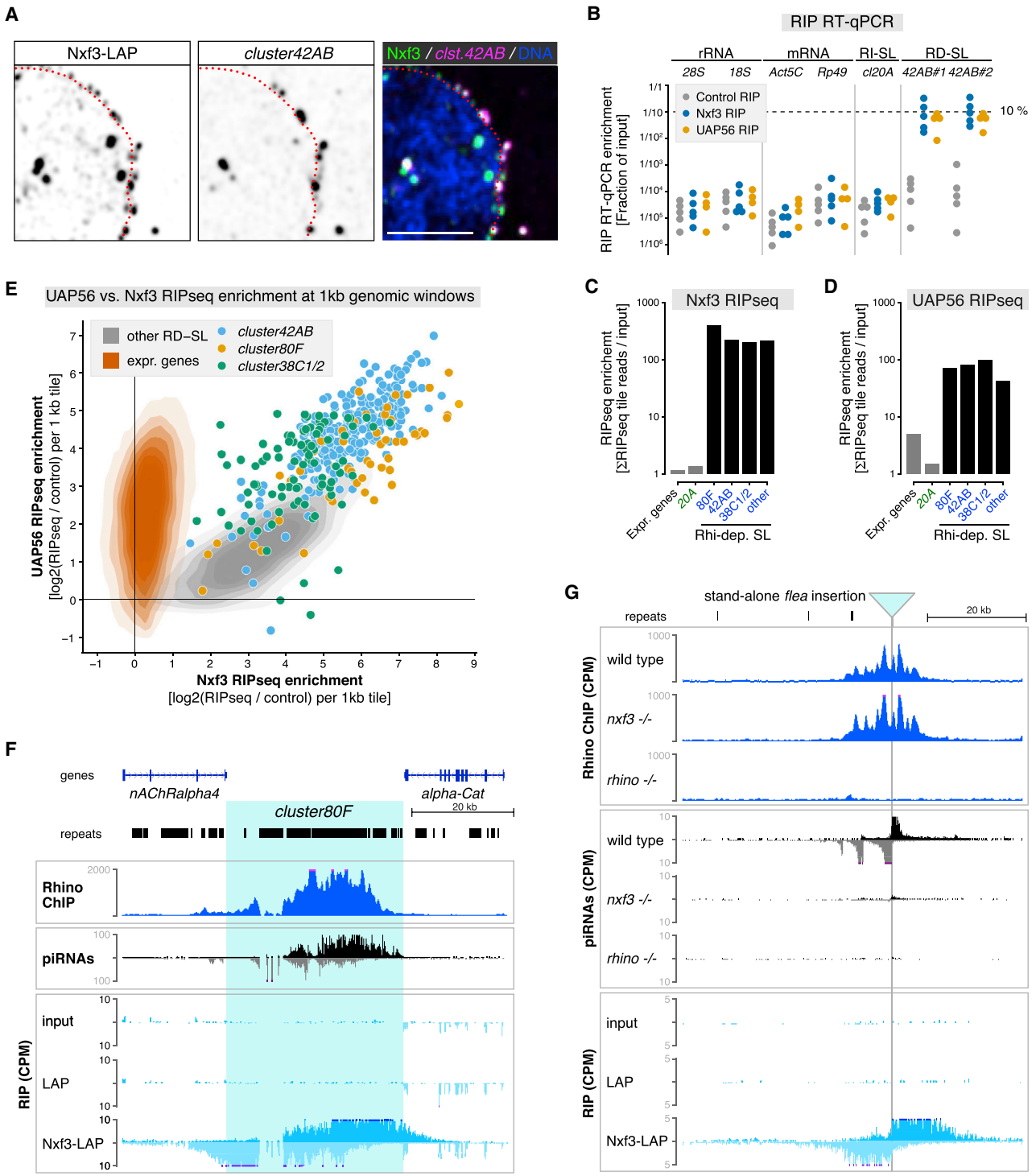

Figure 3. Nxf3 Binds piRNA Precursors

(A) Confocal image showing co-localization of Nxf3-LAP with *cluster42AB* transcripts in nucleus and nuage (dotted line: nuclear envelope; scale bar: 5 μm).

(B) Percentage-input values for indicated transcripts present in control-, Nxf3-, or UAP56-RIP eluates determined by qRT-PCR (dots represent independent experiments).

(C and D) Fold-enrichment values for indicated transcripts in Nxf3- (C) or UAP56- (D) RIP eluates relative to input (based on uniquely mapping reads from RIP-seq libraries).

(legend continued on next page)

enriched for bottom strand precursors, while the last third was enriched for top strand precursors (Figure 3F). This pattern is consistent with a model, where high Rhino levels within the cluster drive bidirectional transcription initiation through Moonshiner, and divergent transcription extends for several kilobases (Andersen et al., 2017). At standalone transposon insertions, which often act as Rhino-dependent mini-clusters (Mohn et al., 2014; Shpiz et al., 2014), Nxf3 similarly associated with divergent transcripts that bleed into flanking genomic regions from the transposon insertion site (Figure 3G). Rhino occupancy at such transposon insertions was unchanged in *nxf3* mutants, yet piRNA production (as inferred from piRNAs mapping uniquely to the transposon-flanking regions) was lost. We conclude that Nxf3 associates specifically with transcripts originating from Rhino-bound loci genome-wide.

CG13741/Bootlegger Recruits Nxf3 to piRNA Clusters

To uncover the molecular basis of Nxf3's specificity for Rhino-dependent piRNA precursors, we immuno-purified Nxf3-LAP from ovary lysates and identified co-eluting proteins via quantitative mass spectrometry. Besides Nxt1, two additional factors, UAP56 and the uncharacterized protein CG13741, were highly enriched in Nxf3 immuno-precipitates (Figure 4A). In *uap56[28/sz15]* mutants, an allelic combination that specifically prevents UAP56 localization to Rhino-dependent clusters but not its function in mRNA export (Meignin and Davis, 2008; Zhang et al., 2012), Nxf3 levels were reduced (Figure 4B), supporting a functional link between these two factors. However, as UAP56 binds Nxf3-dependent piRNA precursors as well as Nxf1-dependent mRNAs (Figure 3E), it is unlikely to determine Nxf3 specificity. In support of this, *uap56[28/sz15]* mutant germline cells still displayed co-localization of the remaining Nxf3 with Rhino in discrete nuclear foci (Figure 4C).

The other Nxf3 interactor, CG13741, was previously identified as a putative piRNA pathway factor in a genetic transposon derepression screen (Czech et al., 2013). CG13741 lacks recognizable protein domains and is preferentially expressed in ovaries (Brown et al., 2014) (Figure S5A). Using CRISPR-Cas9, we inserted a LAP tag at the C terminus of the endogenous *CG13741* locus. Imaging of ovaries from CG13741-LAP flies revealed that CG13741 exhibits a dual subcellular localization indistinguishable from that of Nxf3 (Figure 4D), with the nuclear signal corresponding to piRNA clusters (Rhino-positive), and the cytoplasmic signal corresponding to nuage (Vasa-positive; Figure 4E).

To test whether CG13741 is important for Rhino-dependent piRNA clusters and Nxf3 function, we generated *CG13741* frameshift-null alleles (Figures S5B and S5C). Like *rhino* and *nxf3* mutants, *CG13741* mutants were viable yet female sterile and exhibited loss of piRNAs specifically from Rhino-dependent piRNA source loci (Figure 4F). Consequently, antisense piRNAs targeting germline transposons were reduced (Figure 4G; Figure S5D) and several transposons (e.g., *HMS-Beagle*, *blood*, *HeT-A*, *burdock*) were strongly de-silenced, while mRNA expression was globally unperturbed (Figure 4H; Figure S5E). These findings defined CG13741 as a piRNA pathway-specific factor with an essential function at Rhino-dependent piRNA clusters in conjunction with Nxf3.

We next determined the genetic dependency between CG13741 and Nxf3. In *CG13741* mutants, Nxf3 protein levels were reduced and remaining Nxf3 showed no enrichment at nuclear Rhino-foci, which remained prominent throughout oogenesis in the absence of CG13741 (Figures 5A and 5B). These data pointed to a recruitment hierarchy of Nxf3-associated proteins to Rhino-dependent piRNA source loci. We therefore systematically probed the localization of Nxf3, CG13741, Nxt1, Rhino, Cutoff, and Deadlock in ovaries depleted of factors implicated in Rhino biology. Loss of Rhino, Deadlock, or Cutoff (three interdependent proteins co-localizing at nuclear Rhino foci) resulted in reduced levels of Nxf3 and CG13741 proteins (Figure S5F and S5G) and in their dispersal in nuclei (Figures 5C and 5D; Figure S5H). Loss of CG13741 had similar effects on Nxf3, but Rhino, Deadlock, and Cutoff still accumulated together in nuclear foci (Figure 5C; Figure S5I). Loss of Nxf3 instead had no impact on CG13741 localization to Rhino-Deadlock-Cutoff foci in the nucleus (Figure 5D; Figures S5H and S5I). It did, however, prevent the accumulation of Nxt1 at Rhino foci (Figure 5E). Together, these data placed CG13741 downstream of Rhino-Deadlock-Cutoff and upstream of Nxf3-Nxt1 in the nuclear recruitment hierarchy to piRNA clusters. Due to its central role in nuclear export of piRNA precursors—products of Moonshiner-mediated transcription within heterochromatin—we named CG13741 Bootlegger.

To understand how Bootlegger connects to the upstream Rhino-Deadlock-Cutoff complex at piRNA clusters, we immuno-purified Bootlegger-LAP from ovary lysates and determined co-eluting proteins with quantitative mass-spectrometry. While this confirmed the interaction between Bootlegger, UAP56, and Nxf3-Nxt1 (Figures 5F and 5G), it did not reveal any link to Rhino-Deadlock-Cutoff. A complementary attempt to identify Bootlegger interactors through a yeast two-hybrid screen failed due to the strong auto-activating character of Bootlegger as bait. We therefore performed a yeast two-hybrid screen with the Rhino-interactor Deadlock, which acts as adaptor protein by recruiting Cutoff and Moonshiner, two effector proteins involved in piRNA cluster transcription (Andersen et al., 2017; Mohn et al., 2014). From an ovarian cDNA library, we recovered more than a dozen clones each for the previously identified Deadlock-interactors Rhino and Cutoff (Figure S5J). Notably, >100 sequenced clones represented Bootlegger fragments, all of which shared an ~100 amino acid peptide at the C terminus. The C-terminal Bootlegger fragment interacted

(E) Enrichments (relative to input) of Nxf3- versus UAP56 RIP-seq reads mapping to 1-kb tiles overlapping expressed gene loci (orange; n > 25,000) or to 1-kb tiles overlapping Rhino-dependent piRNA source loci (gray; n = 2,996; 1-kb tiles mapping to major piRNA clusters are colored).

(F and G) UCSC genome browser panels showing Rhino ChIP-seq reads, piRNAs, and RIP-seq reads from control (LAP) and Nxf3-LAP eluates mapping to *cluster80F* (F) or a standalone *flea* transposon insertion (G) (not present in reference genome). CPM, coverage per million reads; piRNA coverage normalized to miRNA reads.

See also Figure S4.

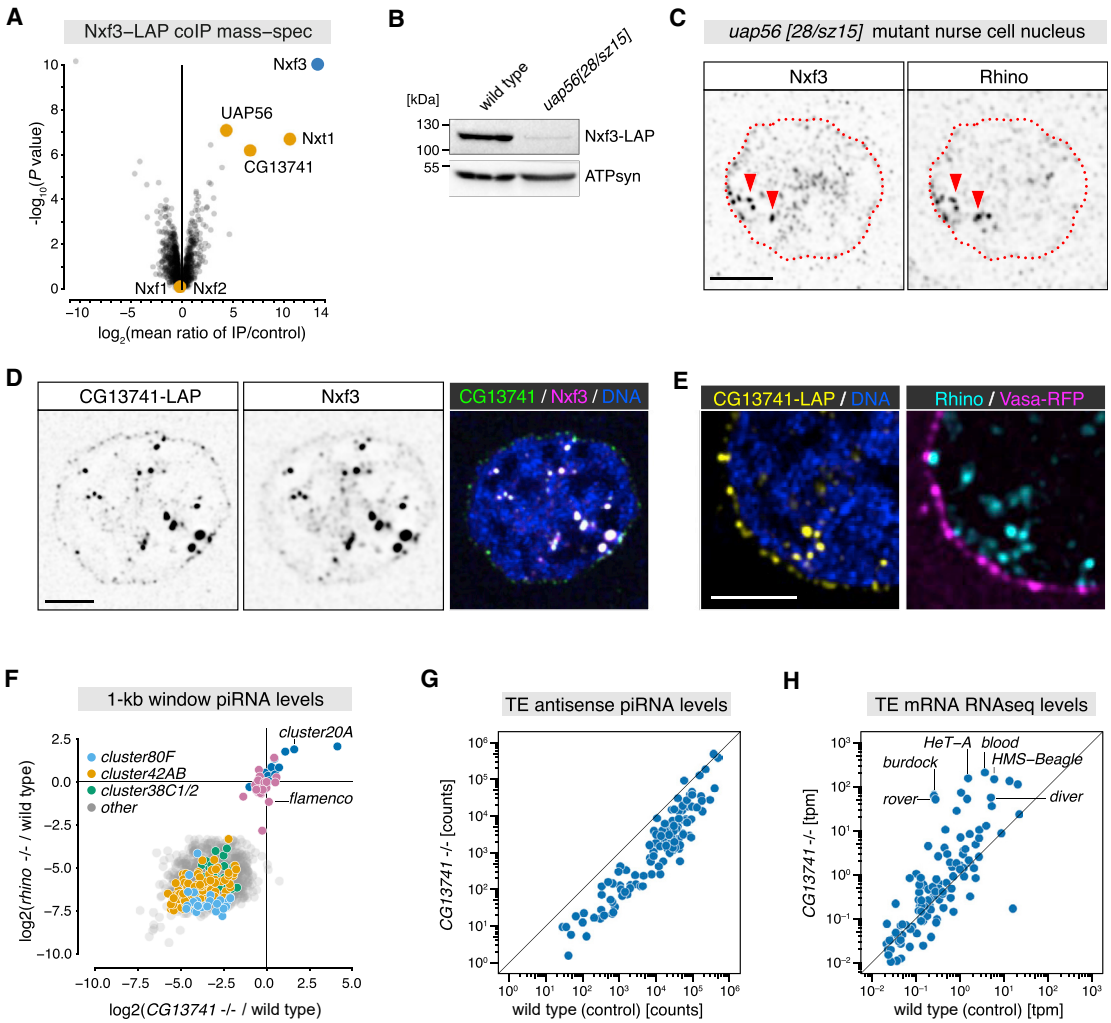

Figure 4. CG13741/Bootlegger and Nxf3 Are Physically and Functionally Connected

(A) Enrichment values and corresponding significance levels for proteins co-purifying with Nxf3-LAP versus control (nuclear LAP) from ovary lysates (n = 4).

(B) Western blot indicating Nxf3-LAP levels in control versus *uap56* mutant ovary lysates (ATP-synthase: loading control).

(C) Nxf3-LAP and Rhino localization in nurse cell nucleus of a *uap56* mutant ovary (scale bar: 5 μm; dotted line: nuclear envelope).

(D) Confocal images showing a nurse cell nucleus (scale bar: 5 μm) indicating co-localization of CG13741-LAP and Nxf3 (antibody stained; Nxf3 in nuage foci is less efficiently detected using antibodies compared to the signal from Nxf3-LAP).

(E) Part of a nurse cell nucleus indicating localization of CG13741-LAP, Rhino, and mCherry-Vasa (scale bar: 5 μm).

(F) log2 fold changes of piRNAs mapping uniquely to 1-kb tiles from Rhino-dependent piRNA clusters in *rhino* versus *CG13741* mutants (relative to control). Tiles from major piRNA clusters are colored; *cluster20A* and *flamenco* tiles serve as Rhino-independent control group.

(G and H) Levels of antisense piRNAs (G) or sense mRNA reads (H) mapping to consensus transposon sequences from control versus *CG13741* mutant samples. See also Figure S5.

specifically with the structured, C-terminal part of Deadlock, the same protein fragment that also binds Cutoff (Figure 5H) (Andersen et al., 2017; Mohn et al., 2014). This established a direct molecular link between Bootlegger and Deadlock and thereby the Rhino-Deadlock-Cutoff complex that defines heterochromatic piRNA clusters.

Nxf3 and Bootlegger associate with the general mRNA export factor UAP56 (Figures 4A and 5F). We therefore extended our genetic hierarchy experiments and asked whether Nxf3 or Bootlegger also contribute to the recruitment of UAP56 to Rhino-dependent piRNA clusters. Depleting Bootlegger, but not Nxf3, led to a loss of UAP56 enrichment at Rhino foci (Figure S5K). Conversely, in *uap56[28/sz15]* mutants, Bootlegger and Nxf3 levels were diminished, yet both proteins still localized to nuclear Rhino foci (Figures 4B and 4C; Figures S5L–S5M). Bootlegger is therefore required for UAP56 to localize to piRNA clusters. Together with published data, this suggests that UAP56 recruitment to Rhino-Deadlock-Cutoff requires two molecular interactions, one via Bootlegger and one via the THO complex (Zhang et al., 2018), which is recruited to Rhino-Deadlock-Cutoff via Cutoff (Hur et al., 2016). Considering that, in *uap56[28/sz15]* mutants, the qualitative pattern of Rhino's chromatin occupancy is

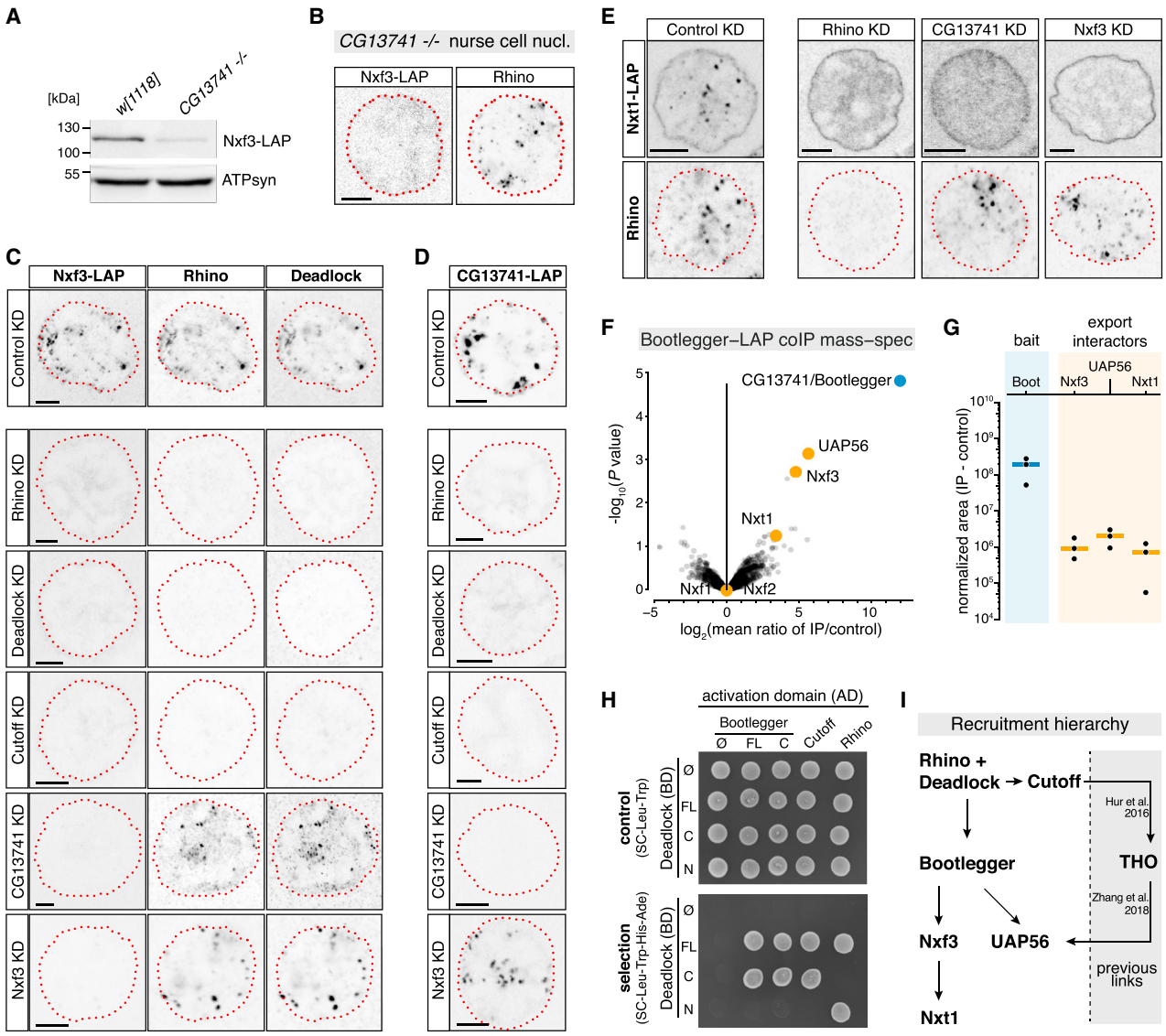

Figure 5. CG13741/Bootlegger Recruits Nxf3 to piRNA Clusters

(A) Western blot indicating Nxf3-LAP levels in control versus *CG13741* mutant ovary lysates (ATP-synthase: loading control).

(B–E) Protein localization in representative nurse cell nuclei displaying Nxf3-LAP and Rhino in *CG13741* mutant ovaries (B), Nxf3-LAP (C), CG13741-LAP (D), or Nxt1-LAP (E) as well as Rhino and Deadlock in ovaries expressing sh-lines targeting indicated genes (KD, knockdown; scale bar: 5 μm; dotted line: nuclear envelope based on DAPI signal, C–E, or wheat germ agglutinin [WGA], B).

(F) Enrichment values and corresponding significance levels for proteins co-purifying with CG13741-LAP versus control (nuclear LAP) from ovaries (n = 3).

(G) Peptide peak intensities (experiment minus respective replicate control) for the CG13741-LAP bait and the proteins indicated in (F) (bars: median values).

(H) Yeast two-hybrid assay on nonselective (top) and selective medium (bottom). AD, Gal4 activation domain; BD, Gal4 DNA binding domain; FL, full-length; C, C-terminal region; N, N-terminal region.

(I) Nuclear recruitment hierarchy of indicated proteins to piRNA clusters, including links from the literature.

See also Figure S5.

changed (Zhang et al., 2018), our findings are in line with the stronger phenotype of *bootlegger* versus *nxf3* mutants in respect to piRNA levels and transposon de-repression (Figures 2D and 2E versus 4G and 4H). Altogether, our data imply that Rhino, via Deadlock, recruits Bootlegger, which in turn recruits Nxf3-Nxt1 and UAP56 to piRNA source loci, thereby specifying the piRNA precursor export pathway (Figure 5I).

Nxf3 Mediates piRNA Precursor Export via Crm1

Besides their differing RNA cargo specificity, a second intriguing discrepancy between Nxf3 and the mRNA export receptor Nxf1 is their respective fate after NPC passage. Nxf1 is actively stripped off its RNA cargo right after it reaches the cytoplasmic side of the NPC (Köhler and Hurt, 2007; Lund and Guthrie, 2005). This dissociation is thought to prevent re-import of mRNA into the

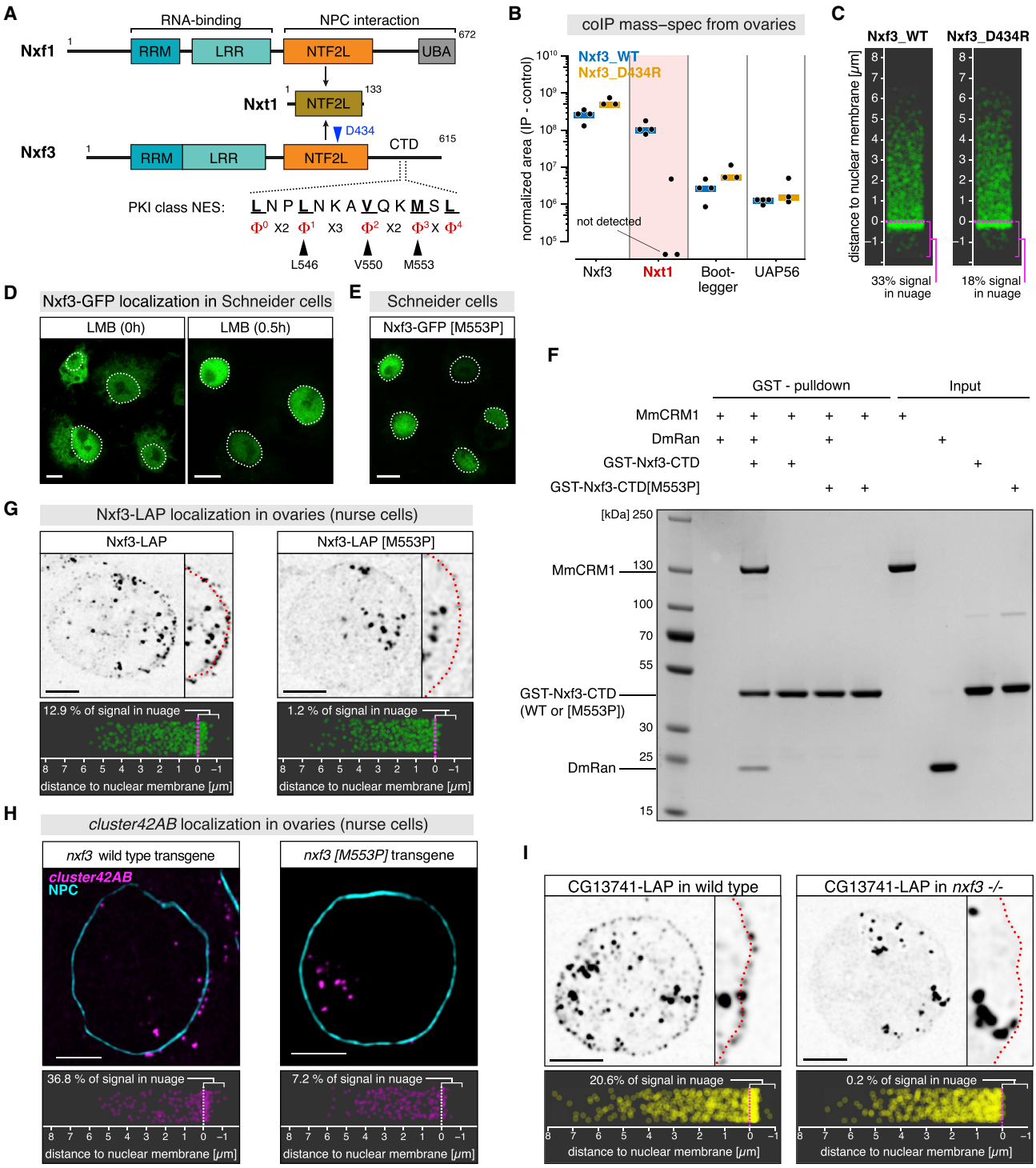

Figure 6. Nxf3 Utilizes Crm1 for Nuclear Export

(A) Protein domain composition of Nxf1, Nxf3, and Nxt1 (RRM, RNA binding motif; LRR, leucine-rich repeat; NTF2-like domain; UBA, ubiquitin-associated domain; CTD, C-terminal domain). The PKI type NES in Nxf3 is indicated.

(B) Absolute peptide peak intensities for indicated Nxf3 interactors from co-immuno-precipitation of wild-type Nxf3-LAP (WT) and Nxt1-interaction mutant Nxf3-LAP (D434R).

(C) Positions of Nxf3-LAP foci in nurse cells relative to nuclear envelope (n = 1,500 foci; see Figure S6F for representative confocal image).

(D) Confocal images showing sub-cellular localization of Nxf3-GFP in untreated (left) or LMB-treated (right) S2 cells (scale bar: 5 μm).

(E) Confocal image showing sub-cellular localization of Nxf3-GFP [M553P] (see A) in S2 cells (scale bar: 5 μm).

(legend continued on next page)

nucleus and thereby confers directionality to mRNA export. Consistent with this, immunofluorescence experiments (Figure 1D) and immuno-gold electron microscopy (Figure S6A) detected Nxf1 enriched at the nuclear envelope, but not in the cytoplasm. In contrast, Nxf3 is enriched together with piRNA precursors in nuage, a cytoplasmic RNA processing granule (Figure 1H; Figure S1G). This suggested a fundamentally different export mechanism for Nxf3 that ensures transport directionality despite Nxf3 remaining bound to its RNA cargo after NPC passage.

To understand how Nxf3 achieves nuclear export, we compared it to Nxf1, which harbors two nucleoporin binding sites that act synergistically to promote NPC translocation (Braun et al., 2002; Fribourg et al., 2001). The first site is formed by Nxf1's ubiquitin-associated domain (UBA). Nxf3 lacks a recognizable UBA domain and this nucleoporin binding site is therefore absent (Figure 6A; Figure S6B). Nxf1's second nucleoporin binding site is formed by the NTF2-like domain, which binds to Nxt1. Nxf1-Nxt1 hetero-dimerization via this interaction is required for Nxf1's nuclear shuttling ability (Katahira et al., 2002; Lévesque et al., 2001). We therefore investigated Nxt1's role in Nxf3 export. Using a heterologous co-immuno-precipitation assay in Schneider cells, we verified that Nxt1 binds Nxf3's NTF2-like domain (Figure S6C). This interaction was lost upon mutation of Asp-434 (D434), whose equivalent residue in Nxf1 forms a conserved salt bridge to Nxt1 (Figure S6C) (Kerkow et al., 2012). We engineered the D434R allele in the endogenous, LAP-tagged *nxf3* locus of flies. Nxf3[D434R] accumulated at reduced levels *in vivo* and was unable to bind Nxt1 above background (Figure 6B; Figure S6D). However, Nxf3[D434R] still interacted with UAP56 and Bootlegger (Figure 6B), co-localized with Rhino at piRNA clusters in the nucleus (Figure S6E), and was enriched in cytoplasmic nuage albeit to a slightly reduced extent (Figure 6C; Figure S6F). *nxf3[D434R]* mutants were, however, sub-fertile and exhibited transposon de-silencing (Figure S6G). Consistent with this, nuage-localized *cluster42AB* transcripts and piRNAs from Rhino-dependent source loci were reduced in *nxf3[D434R]* mutants (Figures S6H and S6I). Besides stabilizing Nxf3, Nxt1 might therefore contribute to RNA cargo binding, similar to what is known for Nxf1-Nxt1 (Aibara et al., 2015; Katahira et al., 2015). Altogether, our data demonstrate that Nxt1 is important for Nxf3 function and suggest that Nxf3 achieves nuclear export independent of nucleoporin binding sites that are critical for Nxf1.

Human NXF3, an orphan NXF variant that despite the identical name arose through duplication independent of *Drosophila* Nxf3 (Stutz and Izaurralde, 2003), achieves NPC translocation via a leucine-rich nuclear export signal (NES) that is recognized by Crm1, the principal cellular exportin (Yang et al., 2001). When expressed in S2 cells, *Drosophila* Nxf3 localized to cytoplasm and nucleus (Figure 6D), but it was entirely nuclear upon treating S2 cells with the Crm1 inhibitor Leptomycin B (LMB) (Figure 6D) (Kudo et al., 1999). Similar results were obtained with endogenous Nxf3 in LMB-treated ovaries (Figure S7A). We identified a candidate NES in Nxf3's C-terminal domain (CTD). Indeed, the presumably unstructured CTD of Nxf3, when fused to GFP, rendered the nuclear localization of GFP LMB dependent (Figure S7B). Nxf3's putative NES sequence is conserved among *Drosophilids* and matches all criteria of a PKI-type NES (Figure 6A; Figure S6B) (Güttler et al., 2010). Two independent point mutations in this NES (construct 1: L546A + V550A; construct 2: M553P) rendered full-length Nxf3 or the CTD entirely nuclear in S2 cells (Figures 6A and 6E; Figures S7C and S7D), supporting a role for this sequence motif as a bona fide NES. Indeed, Nxf3's CTD bound Crm1 in a RanQ69L-dependent manner *in vitro*, and this interaction was abolished in the M553P point mutant (Figure 6F). We did not succeed in generating flies with NES mutations in the endogenous *nxf3* locus, and therefore complemented *nxf3* mutants with a germline-expressed *nxf3* cDNA construct carrying the M553P mutation. Nxf3[M553P] localized to nuclear Rhino foci (Figure 6G) was expressed at levels comparable to the ectopically expressed wild-type protein (Figure S7E) but did not accumulate efficiently in cytoplasmic nuage (Figure 6G). Similarly, *cluster42AB* transcripts accumulated only weakly in nuage of *nxf3[M553P]* mutant ovaries (Figure 6H). These findings demonstrate that Nxf3 utilizes an NES in order to achieve nuclear export via Crm1. *nxf3[M553P]* mutant flies exhibited strong sterility only after ~5 days (Figure S7F). This milder phenotype compared to the *nxf3*-null mutant may be connected to the observation that Crm1-RanQ69L exhibited weak residual binding to the Nxf3 CTD[M553P] peptide *in vitro* (Figure 6F).

Our data reveal that Nxf3, rather than using direct nucleoporin-binding sites like Nxf1, has evolved an NES in order to tap into the Crm1-dependent nuclear export system. Remarkably, in *nxf3* mutants where Vasa-positive nuage granules remain abundant (Figure S7G), Bootlegger is entirely nuclear and fails to enrich in nuage (Figure 6I). Thus, by utilizing the Crm1 system, Nxf3 achieves export not only for its RNA cargo but also for Bootlegger. We speculate that this allows Nxf3-Bootlegger to direct piRNA precursors to nuage, where PIWI-clade proteins loaded with complementary piRNAs will initiate piRNA biogenesis (Han et al., 2015; Homolka et al., 2015; Mohn et al., 2015; Webster et al., 2015).

DISCUSSION

In this work, we uncover the Nxf3-Bootlegger pathway, which transports RNA Polymerase II-generated transcripts emanating

(F) Coomassie stained SDS-PAGE gel showing *in vitro* binding assay of indicated GST-tagged Nxf3-CTD peptides, MmCRM1, and DmRanQ69L.
(G) Confocal images (scale bar: 5 μm; dotted line: nuclear envelope) showing localization of Nxf3-LAP (left) or Nxf3-LAP [M553P] (right) in nurse cells (Nxf3-LAP expressed under *nanos* promoter in *nxf3* mutant). Jitter plots indicate distance of respective protein foci to nuclear envelope (n = 501 foci analyzed per genotype).
(H) Confocal images (scale bar: 5 μm) of nurse cells expressing Nxf3-LAP (left) or Nxf3-LAP [M553P] (right) stained for *cluster42AB* transcripts (magenta) and nuclear pores (WGA: cyan). Jitter plots show positions of *cluster42AB* FISH foci in nurse cells of indicated genotype relative to nuclear envelope (n = 223 foci).
(I) Confocal images of representative nurse cell nuclei (scale bar: 5 μm; magnified panels show part of nucleus; dotted line: nuclear envelope) showing localization of Bootlegger. Jitter plots indicate the distance of Bootlegger foci to nuclear envelope (n = 572 foci analyzed per genotype).
See also Figure S6.

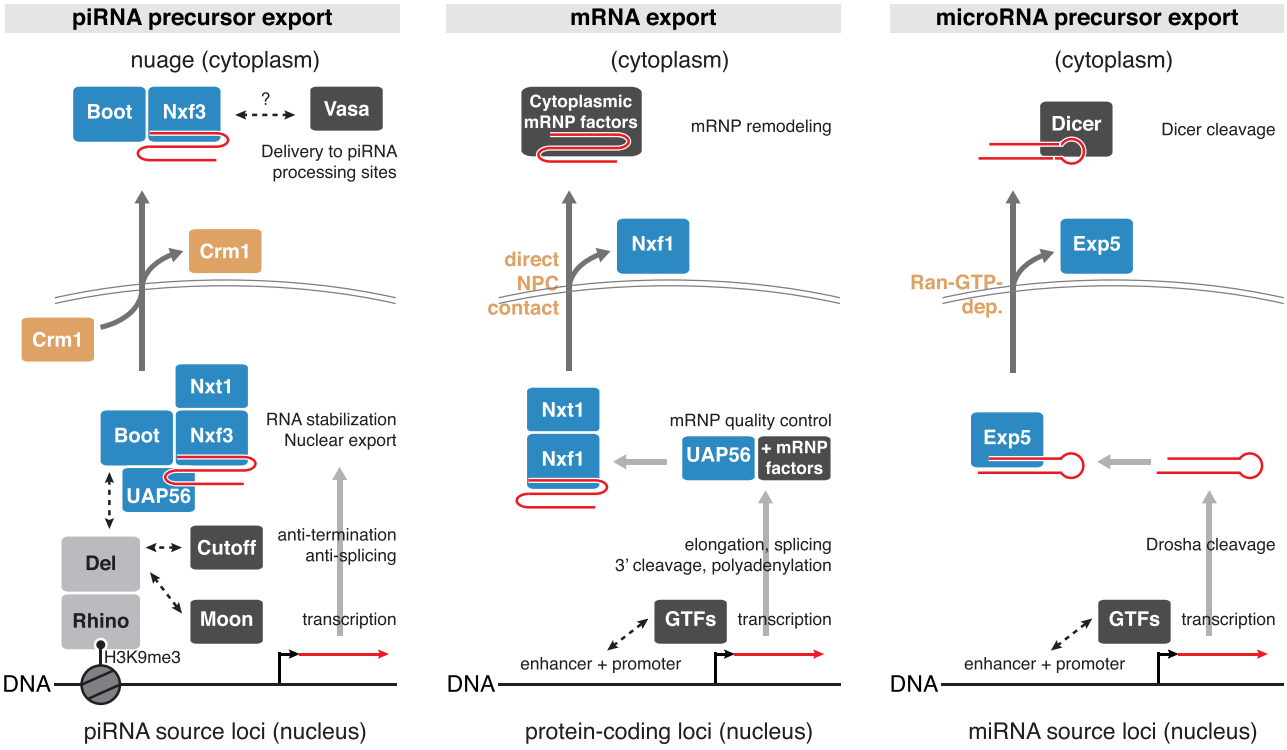

Figure 7. Comparison of Nuclear RNA Export Pathways

Schematics of the Nxf3-Bootlegger pathway in comparison to mRNA export and pre-miRNA export (GTF, general transcription factors).

from heterochromatin to peri-nuclear nuage where they are processed into piRNAs. This pathway (1) bypasses nuclear RNA surveillance mechanisms that would otherwise degrade the unprocessed precursor RNAs and (2) enables nuclear export and delivery of the piRNA precursors to nuage. Retroviruses also must bypass nuclear RNA quality-control mechanisms to export their unprocessed genomic RNA. Specific hairpins in the retroviral RNA recruit the mRNA export receptor Nxf1/Tap (e.g., Mason-Pfizer monkey virus) (Grüter et al., 1998) or exploit the exportin Crm1 through a virally encoded adaptor protein (e.g., HIV) (Cullen, 2000). Due to their high sequence diversity, piRNA precursors are unlikely to recruit export machinery via sequence or structural features. Instead, our work suggests that specificity in piRNA precursor export is achieved through Rhino, which recruits the specialized NXF variant, Nxf3, to nascent transcripts at heterochromatic piRNA clusters. The Nxf3-Bootlegger pathway highlights Rhino's central role in facilitating productive expression of transposon sequence information within heterochromatin (Figure 7). Via its adaptor protein Deadlock, Rhino connects H3K9me3 marks at piRNA clusters to a set of effector proteins that allow transcription initiation (through the TFIIA-L paralog Moonshiner), prevents transcription termination (through the Rai1/DXO paralog Cutoff), and directs nuclear export of the emerging unprocessed RNAs (through the Nxf1 paralog Nxf3). In this, Rhino provides an epigenetic specificity anchor at heterochromatic piRNA clusters where the canonical layers of specificity are either inaccessible (transcription factor binding sites for transcription initiation) or absent (RNA maturation signatures for nuclear export). Thus, central dogmas of gene expression control are bypassed at piRNA clusters through the action of physically connected paralogs of core gene expression factors.

Notably, another NXF paralog, *Drosophila* Nxf2, is also an essential piRNA pathway factor as it licenses heterochromatin formation downstream of nuclear Piwi (Batki et al., 2019; Fabry et al., 2019; Murano et al., 2019; Zhao et al., 2019). This points to the NXF protein family as a hotspot for genetic innovation through gene duplication and neo-functionalization. In vertebrates, Nxf1/Tap has also diversified into multiple NXF variants (Stutz and Izaurralde, 2003). Mammalian NXF2 and NXF3 (both not directly related to *Drosophila* Nxf2 and Nxf3) are preferentially expressed in gonads, and *Nxf2* mutant mice are male sterile (Pan et al., 2009). We propose that neo-functionalized NXF variants have evolved throughout the animal kingdom at least in part to serve key functions in genome defense.

In order to modulate gene expression control, neo-functionalized protein paralogs must connect to the central gene expression machinery. Indeed, Nxf3 and Bootlegger co-purify with UAP56, a nuclear DEAD-box ATPase that facilitates loading of Nxf1-Nxt1 onto export-competent mRNA. In the context of mRNA export, UAP56 functions together with the THO complex (Heath et al., 2016; Ren et al., 2017). Recent work indicates a role for UAP56 and THO in piRNA cluster transcription and in defining Rhino's chromatin occupancy (Zhang et al., 2018). Based on our findings, we speculate that UAP56 and THO, analogous to their function in mRNA export, also license loading of Nxf3-Nxt1 onto piRNA precursors. In this process, Bootlegger might function

analogous to SR proteins, canonical export adaptors that recruit Nxf1-Nxt1 to export-competent mRNA (Müller-McNicoll et al., 2016), or analogous to the adaptor Aly/Ref that interacts with UAP56 and Nxf1-Nxt1 (Strässer and Hurt, 2001). We propose that the mechanistic investigation of specialized paralog-based gene expression pathways, such as the Nxf3-Bootlegger pathway, will provide important insight also into the molecular principles of canonical gene expression.

While the Nxf3-Bootlegger pathway evolved from the general mRNA export machinery, it also shares similarities to pre-microRNA export, which is dependent on Exportin-5 (Bohnsack et al., 2004; Lund et al., 2004; Yi et al., 2003) (Figure 7). In both cases, the export machinery not only facilitates passage through the NPC, but binding of the export factors to cargo RNA also protects against nuclear RNA degradation. Similarly, and in contrast to mRNA export, both pathways utilize the Ran-GTP gradient, either directly (Exportin-5) or indirectly via Crm1 (Nxf3). As the Ran-GTP gradient confers directionality to nuclear transport pathways (here via dissociation of Crm1 from Nxf3 in the cytoplasm), we suggest that Crm1-mediated export allows Nxf3 to remain bound to its own RNA cargo after nuclear export. Staying RNA bound enables Nxf3 and Bootlegger to escort piRNA precursors to nuage, a peri-nuclear biomolecular condensate (Nott et al., 2015) where the piRNA biogenesis machinery is concentrated. The identification of the Nxf3-Bootlegger pathway thus provides key insight into the long sought-after mechanism that contributes specificity to piRNA biogenesis. Remarkably, human NXF3 has independently evolved an export dependency on Crm1, suggesting that it also holds on to its RNA cargo after NPC translocation. NXF variants might therefore more broadly enable delivery of RNA cargo to specific subcellular compartments. The Nxf3-Bootlegger pathway provides a glimpse into how biological information is sorted and spatially distributed in cells. We note that similar findings on the Nxf3-Bootlegger pathway have been published by Kneuss and colleagues during the proof stages of this manuscript (Kneuss et al., 2019).

STAR★METHODS

Detailed methods are provided in the online version of this paper and include the following:

- KEY RESOURCES TABLE
- LEAD CONTACT AND MATERIALS AVAILABILITY
- EXPERIMENTAL MODEL AND SUBJECT DETAILS
  - Fly Husbandry
  - Cell lines
- METHOD DETAILS
  - Generation of transgenic fly strains
  - Generation of mutant fly strains
  - Generation of endogenous knock-in fly strains
  - Protein co-immunoprecipitation from S2 cell lysates
  - Western blot analysis
  - Recombinant protein expression and purification
  - Pulldown experiments
  - Electrophoretic mobility shift assay (EMSA)
  - Protein co-immunoprecipitation from ovary lysates
  - Mass Spectrometry Analyses
  - Yeast Two-Hybrid Analysis
  - RT-qPCR analysis of transposon expression
  - Immuno-gold Electron Microscopy
  - Immunofluorescence staining of ovaries
  - Immunofluorescence staining of S2 cells
  - RNA Fluorescent *In Situ* Hybridization (FISH)
  - Imaging data analysis for localization studies
  - Defining and Curating 1 kb Genomic Windows
  - ChIP-Seq library preparation
  - ChIP-Seq Analysis
  - RNA-Seq library preparation
  - RNA-Seq Analysis
  - Small RNA-Seq library preparation
  - Small RNA-Seq Analysis
  - RIP-Seq library preparation
  - RIP-qPCR
  - RIP-Seq analyses
  - PRO-Seq library preparation
  - PRO-Seq analysis
  - NXF family protein sequence alignments
- DATA AND CODE AVAILABILITY
- QUANTIFICATION AND STATISTICAL ANALYSES
- ADDITIONAL RESOURCES

SUPPLEMENTAL INFORMATION

Supplemental Information can be found online at https://doi.org/10.1016/j.cell.2019.07.007.

ACKNOWLEDGMENTS

We thank D. Handler for bioinformatics help, P. Duchek and J. Gokcezade for generating CRISPR-edited and transgenic flies, K. Mechtler and team for mass spectrometry, and M. Novatchkova for protein phylogenetic analysis. The Vienna Biocenter Core Facilities (VBCF) provided Next Generation Sequencing (NGS unit), recombinant protein expression (ProTech), fly husbandry and fly stocks (VDRC), and electron microscopy (EM facility). We thank the IMBA/GMI/IMP BioOptics facility, in particular, P. Pasierbek, for support, the Monoclonal facility at Max Perutz Labs for monoclonal antibodies, L. Baumgartner for help with Y2H experiments, and D. Görlich for the CRM1 expression plasmid and advice. B. Theurkauf, I. Davis, and E. Gavis provided fly lines. We thank T. Heick Jensen, C. Plaschka, and G. Riddihough (https://lifescienceeditors.com) for comments on the manuscript. The Brennecke lab is supported by the Austrian Academy of Sciences, the European Research Council (ERC-2015-CoG - 682181), and the Austrian Science Fund (F 4303 and W1207). P.R.A. is supported by the Novo Nordisk Foundation (NNF14OC0009189 and NNF17OC0030954) and M.F.E. by a DOC Fellowship from the Austrian Academy of Sciences.

AUTHOR CONTRIBUTIONS

M.F.E., L.T., F.P., and P.R.A. performed all molecular biology and fly experiments. U.H. performed *in vitro* Crm1 analysis. K.M. established LAP-tagged fly lines, T.L. and M.F.E. performed the image analysis for sub-cellular protein localization. M.F.E., J.B., and P.R.A. performed the computational analyses. P.R.A. and J.B. supervised the project. M.F.E., P.R.A., and J.B. wrote the paper.

DECLARATION OF INTERESTS

The authors declare no competing interests.

Received: March 11, 2019
Revised: June 18, 2019
Accepted: June 29, 2019
Published: August 8, 2019

REFERENCES

Aibara, S., Katahira, J., Valkov, E., and Stewart, M. (2015). The principal mRNA nuclear export factor NXF1:NXT1 forms a symmetric binding platform that facilitates export of retroviral CTE-RNA. Nucleic Acids Res. *43*, 1883–1893.

Andersen, P.R., Tirian, L., Vunjak, M., and Brennecke, J. (2017). A heterochromatin-dependent transcription machinery drives piRNA expression. Nature *549*, 54–59.

Bartel, P., Chien, C.T., Sternglanz, R., and Fields, S. (1993). Elimination of false positives that arise in using the two-hybrid system. Biotechniques *14*, 920–924.

Batki, J., Schnabl, J., Wang, J., Handler, D., Andreev, V.I., Stieger, C.E., Novatchkova, M., Lampersberger, L., Kauneckaite, K., Xie, W., et al. (2019). The nascent RNA binding complex SFiNX licenses piRNA-guided heterochromatin formation. bioRxiv. https://doi.org/10.1101/609693.

Berrow, N.S., Alderton, D., Sainsbury, S., Nettleship, J., Assenberg, R., Rahman, N., Stuart, D.I., and Owens, R.J. (2007). A versatile ligation-independent cloning method suitable for high-throughput expression screening applications. Nucleic Acids Res. *35*, e45.

Bieniossek, C., Richmond, T.J., and Berger, I. (2008). MultiBac: multigene baculovirus-based eukaryotic protein complex production. Curr. Protoc. Protein Sci *Chapter 5*, Unit 5 20.

Bohnsack, M.T., Czaplinski, K., and Gorlich, D. (2004). Exportin 5 is a RanGTP-dependent dsRNA-binding protein that mediates nuclear export of pre-miRNAs. RNA *10*, 185–191.

Braun, I.C., Herold, A., Rode, M., and Izaurralde, E. (2002). Nuclear export of mRNA by TAP/NXF1 requires two nucleoporin-binding sites but not p15. Mol. Cell. Biol. *22*, 5405–5418.

Brennecke, J., Aravin, A.A., Stark, A., Dus, M., Kellis, M., Sachidanandam, R., and Hannon, G.J. (2007). Discrete small RNA-generating loci as master regulators of transposon activity in Drosophila. Cell *128*, 1089–1103.

Brown, J.B., Boley, N., Eisman, R., May, G.E., Stoiber, M.H., Duff, M.O., Booth, B.W., Wen, J., Park, S., Suzuki, A.M., et al. (2014). Diversity and dynamics of the Drosophila transcriptome. Nature *512*, 393–399.

Chen, Y.A., Stuwe, E., Luo, Y., Ninova, M., Le Thomas, A., Rozhavskaya, E., Li, S., Vempati, S., Laver, J.D., Patel, D.J., et al. (2016). Cutoff Suppresses RNA Polymerase II Termination to Ensure Expression of piRNA Precursors. Mol. Cell *63*, 97–109.

Cullen, B.R. (2000). Nuclear RNA export pathways. Mol. Cell. Biol. *20*, 4181–4187.

Czech, B., Preall, J.B., McGinn, J., and Hannon, G.J. (2013). A transcriptome-wide RNAi screen in the Drosophila ovary reveals factors of the germline piRNA pathway. Mol. Cell *50*, 749–761.

Czech, B., Munafò, M., Ciabrelli, F., Eastwood, E.L., Fabry, M.H., Kneuss, E., and Hannon, G.J. (2018). piRNA-Guided Genome Defense: From Biogenesis to Silencing. Annu. Rev. Genet. *52*, 131–157.

Dennis, C., Brasset, E., Sarkar, A., and Vaury, C. (2016). Export of piRNA precursors by EJC triggers assembly of cytoplasmic Yb-body in Drosophila. Nat. Commun. *7*, 13739.

Dobin, A., Davis, C.A., Schlesinger, F., Drenkow, J., Zaleski, C., Jha, S., Batut, P., Chaisson, M., and Gingeras, T.R. (2013). STAR: ultrafast universal RNA-seq aligner. Bioinformatics *29*, 15–21.

Doblmann, J., Dusberger, F., Imre, R., Hudecz, O., Stanek, F., Mechtler, K., and Durnberger, G. (2018). apQuant: Accurate Label-Free Quantification by Quality Filtering. J. Proteome Res.

Dorfer, V., Pichler, P., Stranzl, T., Stadlmann, J., Taus, T., Winkler, S., and Mechtler, K. (2014). MS Amanda, a universal identification algorithm optimized for high accuracy tandem mass spectra. J. Proteome Res. *13*, 3679–3684.

Durdevic, Z., Pillai, R.S., and Ephrussi, A. (2018). Transposon silencing in the *Drosophila* female germline is essential for genome stability in progeny embryos. Life Sci Alliance *1*, e201800179.

Ejsmont, R.K., Bogdanzaliewa, M., Lipinski, K.A., and Tomancak, P. (2011). Production of fosmid genomic libraries optimized for liquid culture recombineering and cross-species transgenesis. Methods Mol. Biol. *772*, 423–443.

Fabry, M.H., Ciabrelli, F., Munafò, M., Eastwood, E.L., Kneuss, E., Falciatori, I., Falconio, F.A., Hannon, G.J., and Czech, B. (2019). piRNA-guided co-transcriptional silencing coopts nuclear export factors. eLife *8*, e47999.

Fribourg, S., Braun, I.C., Izaurralde, E., and Conti, E. (2001). Structural basis for the recognition of a nucleoporin FG repeat by the NTF2-like domain of the TAP/p15 mRNA nuclear export factor. Mol. Cell *8*, 645–656.

Fromont-Racine, M., Rain, J.C., and Legrain, P. (1997). Toward a functional analysis of the yeast genome through exhaustive two-hybrid screens. Nat. Genet. *16*, 277–282.

Gaspar, I., Wippich, F., and Ephrussi, A. (2017). Enzymatic production of single-molecule FISH and RNA capture probes. RNA *23*, 1582–1591.

Gokcezade, J., Sienski, G., and Duchek, P. (2014). Efficient CRISPR/Cas9 Plasmids for Rapid and Versatile Genome. Editing in Drosophila *4*, 2279–2282.

Goriaux, C., Desset, S., Renaud, Y., Vaury, C., and Brasset, E. (2014). Transcriptional properties and splicing of the flamenco piRNA cluster. EMBO Rep. *15*, 411–418.

Gratz, S.J., Cummings, A.M., Nguyen, J.N., Hamm, D.C., Donohue, L.K., Harrison, M.M., Wildonger, J., and O'Connor-Giles, K.M. (2013). Genome engineering of Drosophila with the CRISPR RNA-guided Cas9 nuclease. Genetics *194*, 1029–1035.

Grüter, P., Tabernero, C., von Kobbe, C., Schmitt, C., Saavedra, C., Bachi, A., Wilm, M., Felber, B.K., and Izaurralde, E. (1998). TAP, the human homolog of Mex67p, mediates CTE-dependent RNA export from the nucleus. Mol. Cell *1*, 649–659.

Güttler, T., Madl, T., Neumann, P., Deichsel, D., Corsini, L., Monecke, T., Ficner, R., Sattler, M., and Görlich, D. (2010). NES consensus redefined by structures of PKI-type and Rev-type nuclear export signals bound to CRM1. Nat. Struct. Mol. Biol. *17*, 1367–1376.

Han, B.W., Wang, W., Li, C., Weng, Z., and Zamore, P.D. (2015). Noncoding RNA. piRNA-guided transposon cleavage initiates Zucchini-dependent, phased piRNA production. Science *348*, 817–821.

Heath, C.G., Viphakone, N., and Wilson, S.A. (2016). The role of TREX in gene expression and disease. Biochem. J. *473*, 2911–2935.

Herold, A., Suyama, M., Rodrigues, J.P., Braun, I.C., Kutay, U., Carmo-Fonseca, M., Bork, P., and Izaurralde, E. (2000). TAP (NXF1) belongs to a multigene family of putative RNA export factors with a conserved modular architecture. Mol. Cell. Biol. *20*, 8996–9008.

Herold, A., Klymenko, T., and Izaurralde, E. (2001). NXF1/p15 heterodimers are essential for mRNA nuclear export in Drosophila. RNA *7*, 1768–1780.

Herold, A., Teixeira, L., and Izaurralde, E. (2003). Genome-wide analysis of nuclear mRNA export pathways in Drosophila. EMBO J. *22*, 2472–2483.

Homolka, D., Pandey, R.R., Goriaux, C., Brasset, E., Vaury, C., Sachidanandam, R., Fauvarque, M.O., and Pillai, R.S. (2015). PIWI Slicing and RNA Elements in Precursors Instruct Directional Primary piRNA Biogenesis. Cell Rep. *12*, 418–428.

Hur, J.K., Luo, Y., Moon, S., Ninova, M., Marinov, G.K., Chung, Y.D., and Aravin, A.A. (2016). Splicing-independent loading of TREX on nascent RNA is required for efficient expression of dual-strand piRNA clusters in Drosophila. Genes Dev. *30*, 840–855.

Jayaprakash, A.D., Jabado, O., Brown, B.D., and Sachidanandam, R. (2011). Identification and remediation of biases in the activity of RNA ligases in small-RNA deep sequencing. Nucleic Acids Res. *39*, e141.

Katahira, J., Straesser, K., Saiwaki, T., Yoneda, Y., and Hurt, E. (2002). Complex formation between Tap and p15 affects binding to FG-repeat nucleoporins and nucleocytoplasmic shuttling. J. Biol. Chem. *277*, 9242–9246.

Katahira, J., Dimitrova, L., Imai, Y., and Hurt, E. (2015). NTF2-like domain of Tap plays a critical role in cargo mRNA recognition and export. Nucleic Acids Res. *43*, 1894–1904.

Kent, W.J., Sugnet, C.W., Furey, T.S., Roskin, K.M., Pringle, T.H., Zahler, A.M., and Haussler, D. (2002). The human genome browser at UCSC. Genome Res. *12*, 996–1006.

Kerkow, D.E., Carmel, A.B., Menichelli, E., Ambrus, G., Hills, R.D., Jr., Gerace, L., and Williamson, J.R. (2012). The structure of the NXF2/NXT1 heterodimeric complex reveals the combined specificity and versatility of the NTF2-like fold. J. Mol. Biol. *415*, 649–665.

Klattenhoff, C., Xi, H., Li, C., Lee, S., Xu, J., Khurana, J.S., Zhang, F., Schultz, N., Koppetsch, B.S., Nowosielska, A., et al. (2009). The Drosophila HP1 homolog Rhino is required for transposon silencing and piRNA production by dual-strand clusters. Cell *138*, 1137–1149.

Kneuss, E., Munafò, M., Eastwood, E.L., Handler, D., Deumer, U., Preall, J.B., Hannon, G.J., and Czech, B. (2019). Specialization of the *Drosophila* nuclear export family protein, Nxf3, for piRNA precursor export. BioRxiv [Preprint]. https://doi.org/10.1101/716258.

Köhler, A., and Hurt, E. (2007). Exporting RNA from the nucleus to the cytoplasm. Nat. Rev. Mol. Cell Biol. *8*, 761–773.

Kudo, N., Matsumori, N., Taoka, H., Fujiwara, D., Schreiner, E.P., Wolff, B., Yoshida, M., and Horinouchi, S. (1999). Leptomycin B inactivates CRM1/exportin 1 by covalent modification at a cysteine residue in the central conserved region. Proc. Natl. Acad. Sci. USA *96*, 9112–9117.

Kwak, H., Fuda, N.J., Core, L.J., and Lis, J.T. (2013). Precise maps of RNA polymerase reveal how promoters direct initiation and pausing. Science *339*, 950–953.

Langmead, B., Trapnell, C., Pop, M., and Salzberg, S.L. (2009). Ultrafast and memory-efficient alignment of short DNA sequences to the human genome. Genome Biol. *10*, R25.

Lee, T.I., Johnstone, S.E., and Young, R.A. (2006). Chromatin immunoprecipitation and microarray-based analysis of protein location. Nat. Protoc. *1*, 729–748.

Lévesque, L., Guzik, B., Guan, T., Coyle, J., Black, B.E., Rekosh, D., Hammarskjöld, M.L., and Paschal, B.M. (2001). RNA export mediated by tap involves NXT1-dependent interactions with the nuclear pore complex. J. Biol. Chem. *276*, 44953–44962.

Lim, A.K., and Kai, T. (2007). Unique germ-line organelle, nuage, functions to repress selfish genetic elements in Drosophila melanogaster. Proc. Natl. Acad. Sci. USA *104*, 6714–6719.

Lund, M.K., and Guthrie, C. (2005). The DEAD-box protein Dbp5p is required to dissociate Mex67p from exported mRNPs at the nuclear rim. Mol. Cell *20*, 645–651.

Lund, E., Güttinger, S., Calado, A., Dahlberg, J.E., and Kutay, U. (2004). Nuclear export of microRNA precursors. Science *303*, 95–98.

Luo, M.L., Zhou, Z., Magni, K., Christoforides, C., Rappsilber, J., Mann, M., and Reed, R. (2001). Pre-mRNA splicing and mRNA export linked by direct interactions between UAP56 and Aly. Nature *413*, 644–647.

Mahat, D.B., Kwak, H., Booth, G.T., Jonkers, I.H., Danko, C.G., Patel, R.K., Waters, C.T., Munson, K., Core, L.J., and Lis, J.T. (2016). Base-pair-resolution genome-wide mapping of active RNA polymerases using precision nuclear run-on (PRO-seq). Nat. Protoc. *11*, 1455–1476.

Mahowald, A.P. (1971). Polar granules of Drosophila. 3. The continuity of polar granules during the life cycle of Drosophila. J. Exp. Zool. *176*, 329–343.

Malone, C.D., Brennecke, J., Dus, M., Stark, A., McCombie, W.R., Sachidanandam, R., and Hannon, G.J. (2009). Specialized piRNA pathways act in germline and somatic tissues of the Drosophila ovary. Cell *137*, 522–535.

Meignin, C., and Davis, I. (2008). UAP56 RNA helicase is required for axis specification and cytoplasmic mRNA localization in Drosophila. Dev. Biol. *315*, 89–98.

Miller, J., and Stagljar, I. (2004). Using the yeast two-hybrid system to identify interacting proteins. Methods Mol. Biol. *261*, 247–262.

Mohn, F., Sienski, G., Handler, D., and Brennecke, J. (2014). The rhino-deadlock-cutoff complex licenses noncanonical transcription of dual-strand piRNA clusters in Drosophila. Cell *157*, 1364–1379.

Mohn, F., Handler, D., and Brennecke, J. (2015). Noncoding RNA. piRNA-guided slicing specifies transcripts for Zucchini-dependent, phased piRNA biogenesis. Science *348*, 812–817.

Morlan, J.D., Qu, K., and Sinicropi, D.V. (2012). Selective depletion of rRNA enables whole transcriptome profiling of archival fixed tissue. PLoS ONE *7*, e42882.

Müller-McNicoll, M., Botti, V., de Jesus Domingues, A.M., Brandl, H., Schwich, O.D., Steiner, M.C., Curk, T., Poser, I., Zarnack, K., and Neugebauer, K.M. (2016). SR proteins are NXF1 adaptors that link alternative RNA processing to mRNA export. Genes Dev. *30*, 553–566.

Murano, K., Iwasaki, Y.W., Ishizu, H., Mashiko, A., Shibuya, A., Kondo, S., Adachi, S., Suzuki, S., Saito, K., Natsume, T., et al. (2019). Nuclear RNA export factor variant initiates piRNA-guided co-transcriptional silencing. bioRxiv. https://doi.org/10.1101/605725.

Ni, J.Q., Zhou, R., Czech, B., Liu, L.P., Holderbaum, L., Yang-Zhou, D., Shim, H.S., Tao, R., Handler, D., Karpowicz, P., et al. (2011). A genome-scale shRNA resource for transgenic RNAi in Drosophila. Nat. Methods *8*, 405–407.

Nott, T.J., Petsalaki, E., Farber, P., Jervis, D., Fussner, E., Plochowietz, A., Craggs, T.D., Bazett-Jones, D.P., Pawson, T., Forman-Kay, J.D., and Baldwin, A.J. (2015). Phase transition of a disordered nuage protein generates environmentally responsive membraneless organelles. Mol. Cell *57*, 936–947.

Ozata, D.M., Gainetdinov, I., Zoch, A., O'Carroll, D., and Zamore, P.D. (2018). PIWI-interacting RNAs: small RNAs with big functions. Nat. Rev. Genet. *20*, 89–108.

Pan, J., Eckardt, S., Leu, N.A., Buffone, M.G., Zhou, J., Gerton, G.L., McLaughlin, K.J., and Wang, P.J. (2009). Inactivation of Nxf2 causes defects in male meiosis and age-dependent depletion of spermatogonia. Dev. Biol. *330*, 167–174.

Pane, A., Jiang, P., Zhao, D.Y., Singh, M., and Schüpbach, T. (2011). The Cutoff protein regulates piRNA cluster expression and piRNA production in the Drosophila germline. EMBO J. *30*, 4601–4615.

Patro, R., Duggal, G., Love, M.I., Irizarry, R.A., and Kingsford, C. (2017). Salmon provides fast and bias-aware quantification of transcript expression. Nat. Methods *14*, 417–419.

Pimentel, H., Bray, N.L., Puente, S., Melsted, P., and Pachter, L. (2017). Differential analysis of RNA-seq incorporating quantification uncertainty. Nat. Methods *14*, 687–690.

Port, F., Chen, H.M., Lee, T., and Bullock, S.L. (2014). Optimized CRISPR/Cas tools for efficient germline and somatic genome engineering in Drosophila. Proc. Natl. Acad. Sci. USA *111*, E2967–E2976.

Preibisch, S., Saalfeld, S., Schindelin, J., and Tomancak, P. (2010). Software for bead-based registration of selective plane illumination microscopy data. Nat. Methods *7*, 418–419.

Quinlan, A.R., and Hall, I.M. (2010). BEDTools: a flexible suite of utilities for comparing genomic features. Bioinformatics *26*, 841–842.

Raney, B.J., Dreszer, T.R., Barber, G.P., Clawson, H., Fujita, P.A., Wang, T., Nguyen, N., Paten, B., Zweig, A.S., Karolchik, D., et al. (2013). Track data hubs enable visualization of user-defined genome-wide annotations on the UCSC Genome Browser. Bioinformatics *30*, 1003–1005.

RCoreTeam (2018). R: A Language and Environment for Statistical Computing.

Reed, R., and Hurt, E. (2002). A conserved mRNA export machinery coupled to pre-mRNA splicing. Cell *108*, 523–531.

Ren, Y., Schmiege, P., and Blobel, G. (2017). Structural and biochemical analyses of the DEAD-box ATPase Sub2 in association with THO or Yra1. eLife *6*, e20070.

Schindelin, J., Arganda-Carreras, I., Frise, E., Kaynig, V., Longair, M., Pietzsch, T., Preibisch, S., Rueden, C., Saalfeld, S., Schmid, B., et al. (2012). Fiji: an open-source platform for biological-image analysis. Nat. Methods *9*, 676–682.

Senti, K.A., Jurczak, D., Sachidanandam, R., and Brennecke, J. (2015). piRNA-guided slicing of transposon transcripts enforces their transcriptional silencing via specifying the nuclear piRNA repertoire. Genes Dev. *29*, 1747–1762.

Shpiz, S., Ryazansky, S., Olovnikov, I., Abramov, Y., and Kalmykova, A. (2014). Euchromatic transposon insertions trigger production of novel Pi- and endo-siRNAs at the target sites in the drosophila germline. PLoS Genet. *10*, e1004138.

Siomi, M.C., Sato, K., Pezic, D., and Aravin, A.A. (2011). PIWI-interacting small RNAs: the vanguard of genome defence. Nat. Rev. Mol. Cell Biol. *12*, 246–258.

Smyth, G.K. (2004). Linear models and empirical bayes methods for assessing differential expression in microarray experiments. Stat. Appl. Genet. Mol. Biol *3*, Article3.

Strässer, K., and Hurt, E. (2001). Splicing factor Sub2p is required for nuclear mRNA export through its interaction with Yra1p. Nature *413*, 648–652.

Stutz, F., and Izaurralde, E. (2003). The interplay of nuclear mRNP assembly, mRNA surveillance and export. Trends Cell Biol. *13*, 319–327.

Tokuyasu, K.T. (1973). A technique for ultracryotomy of cell suspensions and tissues. J. Cell Biol. *57*, 551–565.

Venken, K.J., Carlson, J.W., Schulze, K.L., Pan, H., He, Y., Spokony, R., Wan, K.H., Koriabine, M., de Jong, P.J., White, K.P., et al. (2009). Versatile P[acman] BAC libraries for transgenesis studies in Drosophila melanogaster. Nat. Methods *6*, 431–434.

Vizcaíno, J.A., Csordas, A., del-Toro, N., Dianes, J.A., Griss, J., Lavidas, I., Mayer, G., Perez-Riverol, Y., Reisinger, F., Ternent, T., et al. (2016). 2016 update of the PRIDE database and its related tools. Nucleic Acids Res. *44* (D1), D447–D456.

Vojtek, A.B., and Hollenberg, S.M. (1995). Ras-Raf interaction: two-hybrid analysis. Methods Enzymol. *255*, 331–342.

Wang, L., Dou, K., Moon, S., Tan, F.J., and Zhang, Z.Z. (2018). Hijacking Oogenesis Enables Massive Propagation of LINE and Retroviral Transposons. Cell *174*, 1082–1094.

Webster, A., Li, S., Hur, J.K., Wachsmuth, M., Bois, J.S., Perkins, E.M., Patel, D.J., and Aravin, A.A. (2015). Aub and Ago3 Are Recruited to Nuage through Two Mechanisms to Form a Ping-Pong Complex Assembled by Krimper. Mol. Cell *59*, 564–575.

Wehr, K., Swan, A., and Schüpbach, T. (2006). Deadlock, a novel protein of Drosophila, is required for germline maintenance, fusome morphogenesis and axial patterning in oogenesis and associates with centrosomes in the early embryo. Dev. Biol. *294*, 406–417.

Wickham, H. (2016). ggplot2: Elegant Graphics for Data Analysis (Springer-Verlag).

Wickham, H. (2017). scales: Scale Functions for Visualization.

Yang, J., Bogerd, H.P., Wang, P.J., Page, D.C., and Cullen, B.R. (2001). Two closely related human nuclear export factors utilize entirely distinct export pathways. Mol. Cell *8*, 397–406.

Yi, R., Qin, Y., Macara, I.G., and Cullen, B.R. (2003). Exportin-5 mediates the nuclear export of pre-microRNAs and short hairpin RNAs. Genes Dev. *17*, 3011–3016.

Zhang, F., Wang, J., Xu, J., Zhang, Z., Koppetsch, B.S., Schultz, N., Vreven, T., Meignin, C., Davis, I., Zamore, P.D., et al. (2012). UAP56 couples piRNA clusters to the perinuclear transposon silencing machinery. Cell *151*, 871–884.

Zhang, Z., Wang, J., Schultz, N., Zhang, F., Parhad, S.S., Tu, S., Vreven, T., Zamore, P.D., Weng, Z., and Theurkauf, W.E. (2014). The HP1 homolog rhino anchors a nuclear complex that suppresses piRNA precursor splicing. Cell *157*, 1353–1363.

Zhang, G., Tu, S., Yu, T., Zhang, X.O., Parhad, S.S., Weng, Z., and Theurkauf, W.E. (2018). Co-dependent Assembly of Drosophila piRNA Precursor Complexes and piRNA Cluster Heterochromatin. Cell Rep *24*, 3413–3422.

Zhao, K., Cheng, S., Miao, N., Xu, P., Lu, X., Zhang, Y., Wang, M., Ouyang, X., Yuan, X., Liu, W., et al. (2019). A Pandas complex adapted for piRNA-guided transposon silencing. bioRxiv. https://doi.org/10.1101/608273.

STAR★METHODS

KEY RESOURCES TABLE

REAGENT or RESOURCE	SOURCE	IDENTIFIER
Antibodies		
Anti-Actin antibody produced in rabbit	Sigma Aldrich	Cat# A2066; RRID:AB_476693
Anti-ATP5A antibody [15H4C4] produced in mouse	Abcam	Cat# ab14748; RRID:AB_301447
Anti-GFP Living Colors A.v. Monoclonal Antibody (JL-8) produced in mouse	Takara	Cat# 632381; RRID:AB_2313808
Monoclonal ANTI-FLAG M2 antibody produced in mouse	Sigma Aldrich	Cat# F3165-.2MG; RRID:AB_259529
Anti-Rhino polyclonal antibody produced in Rabbit	Mohn et al., 2014	Anti-Rhino_3573 gly; RRID:AB_2568876
Anti-Deadlock monoclonal antibody produced in mouse	Andersen et al., 2017	Anti-Deadlock_5B5; RRID:AB_2568875
Anti-Nxf3 monoclonal antibody produced in mouse	This study	Anti-Nxf3_8E4-F1
Anti-CG13741 monoclonal antibody produced in mouse	This study	Anti-CG13741_8C5-D10
Anti-Mouse IgG (whole molecule)–Peroxidase antibody produced in rabbit	Sigma Aldrich	Cat# A9044-2ML; RRID:AB_258431
Anti-Rabbit IgG (whole molecule)–Peroxidase antibody produced in goat	Sigma Aldrich	Cat# A0545-1ML; RRID:AB_257896
Goat anti-Mouse IgG (H+L) Cross-Adsorbed Secondary Antibody, Alexa Fluor 568	Thermo Fisher Scientific	Cat# A-11004; RRID:AB_2534072
Goat anti-Rabbit IgG (H+L) Cross-Adsorbed Secondary Antibody, Alexa Fluor 568	Thermo Fisher Scientific	Cat# A-11011; RRID:AB_143157
Goat anti-Mouse IgG (H+L) Cross-Adsorbed Secondary Antibody, Alexa Fluor 647	Thermo Fisher Scientific	Cat# A-21235; RRID:AB_2535804
Anti-Nuclear Pore Complex Proteins antibody [Mab414] - ChIP Grade	Abcam	Cat# ab24609; RRID:AB_448181
Chemicals, Peptides, and Recombinant Proteins		
Wheat Germ Agglutinin, Alexa Fluor 647 Conjugate	Thermo Fisher Scientific	Cat# W32466
Wheat Germ Agglutinin, Alexa Fluor 488 Conjugate	Thermo Fisher Scientific	Cat# W11261
RNase OUT	Thermo Fisher Scientific	Cat# 10777-019
Schneider's Drosophila Media	Thermo Fisher Scientific	Cat# 21720001
Trizol Reagent	Life Technologies	Cat# 15596026
Pefabloc SC	Sigma Aldrich	Cat# 11429868001
cOmplete EDTA-free protease inhibitor cocktail tablet	Roche	Cat# 11873580001
Imidazole	Sigma Aldrich	Cat# I5513
Glutathione Sepharose 4B beads	GE Healthcare	Cat# 17075601
Anti-FLAG M2 Magnetic Beads	Sigma Aldrich	Cat# M8823-1ML
L-Glutathione reduced	Sigma Aldrich	Cat# G4251
RQ1 RNase-free DNase	Promega	Cat# M6101
Superscript II	Invitrogen	Cat# 18064014
GoTaq qPCR Master Mix	Promega	Cat# A6001
RNase free Nuclease-free water	Ambion	Cat# AM9932
16% Formaldehyde (w/v), Methanol-free	Thermo Fisher Scientific	Cat# 28906
TetraSpeck™ microspheres, 0.5 μm, fluorescent blue/green/orange/dark red	Invitrogen	Cat# T7281
Leptomycin B solution from Streptomyces sp	Sigma Aldrich	Cat# L2913-5UG
ProLong Diamond Antifade Mountant	Thermo Fisher Scientific	Cat# P36961
Formamide, Molecular Biology Grade	Merck	Cat# 344206-1L
Dextran sulfate	Sigma	Cat# D8906-50G
Dynabeads Protein G for Immunoprecipitation	Thermo Fisher Scientific	Cat# 10004D
Dynabeads Protein A for Immunoprecipitation	Thermo Fisher Scientific	Cat# 10002D

(*Continued on next page*)

Continued

REAGENT or RESOURCE	SOURCE	IDENTIFIER
RNase A, DNase and protease-free	Thermo Fisher Scientific	Cat# EN0531
Hybridase thermostabile RNase H	Biozym Scientific GmbH	Cat# 108211
T4 RNA ligase	NEB	Cat# M0204L
T4 RNA Ligase 2, truncated K227Q	NEB	Cat# M0373L
Triton X-100	Calbiochem	Cat# 9410
Nonidet P40 (NP40) substitute	Sigma Aldrich	Cat# 11332473001
Sarkosyl	Sigma Aldrich	Cat# L5125
Tween-20	Sigma Aldrich	Cat# P9416
Biotin-11-CTP	PerkinElmer	Cat# NEL542001EA
Biotin-11-UTP	PerkinElmer	Cat# NEL543001EA
Tobacco acid pyrophosphatase (TAP)	Epicenter	Cat# T19500
RNaseOUT Recombinant Ribonuclease Inhibitor	Thermo Fisher Scientific	Cat# 10777019
T4 polynucleotide kinase (PNK)	NEB	Cat# M0201
GlycoBlue Coprecipitant	Thermo Fisher Scientific	Cat# AM9515
Dynabeads MyOne Streptavidin C1	Invitrogen	Cat# 65002
Agencourt AMPure XP	Beckman Coulter	Cat# A63880
RNA 5′ Pyrophosphohydrolase (RppH)	NEB	Cat# M0356S
KAPA Hotstart Realtime master mix	Roche	Cat# KK2702
Critical Commercial Assays		
HisTrap HP 5 ml column	GE Healthcare	Cat# 17524802
HisTrap FF 5 ml colum	GE Healthcare	Cat# 17525501
HiTrap Q HP 5 ml column	GE Healthcare	Cat# 17115401
HiTrap SP HP 5 ml column	GE Healthcare	Cat# 17115201
HiLoad 16/600 Superdex 200 pg	GE Healthcare	Cat# 28989335
Cell Line Nucleofector kit V	Amaxa Biosystems	Cat# VVCA-1003
ChIP DNA Clean & Concentrator w/ Zymo-Spin IC Columns (Capped)	Zymo Research	Cat# D5205
RNA RNA Clean & Concentrator -5 w/ Zymo-Spin IC Columns (Capped)	Zymo Research	Cat# R1016
NEBNext Ultra II Directional RNA Library Prep Kit for Illumina	NEB	Cat# E7760L
NEBNext Ultra II DNA Library Prep Kit for Illumina	NEB	Cat# E7645L
RNeasy Mini Kit	QIAGEN	Cat# 74104
Oligonucleotides		
Primers, CRISPR targetting, and shRNA oligonucleotides are listed in Table S2	This study	N/A
RNA-FISH probe set are listed in Table S3	This study	N/A
Antisense rRNA oligos are listed in Table S4	This study	N/A
Deposited Data		
High-throughput sequencing data	This study	GEO: GSE126578
Mass spectrometry data	This study	PRIDE: PXD012717
Bacterial Strains		
Escherichia coli (*E. coli*) strain Rosetta2 (DE3) pLysS	Novagen	N/A
Escherichia coli (*E. coli*) strain DH5α	ThermoFisher	N/A
Experimental Models: Cell Lines		
D. melanogaster: Cell line S2	Phil Zamore lab	N/A
Experimental Models: Organisms/Strains		
D. melanogaster: See Table S1 for all Fly strains used in this study	This study	N/A
S. cerevisiae: See Table S7 for all Yeast strains used in this study	This study	N/A

(*Continued on next page*)

Continued

REAGENT or RESOURCE	SOURCE	IDENTIFIER
Recombinant DNA		
pOPIN-B_6xHis-3C-DmRan, res. 1-180, Q69L	This study	pUH43
pTG-A20_10xHis-zz-TEV-MmCRM1	Güttler et al., 2010	pTG-A20
pGEX-6P-1_GST-3C-DmNxf3, res. 488-615	This study	N/A
pGEX-6P-1_GST-3C-DmNxf3, res. 488-615, M553P	This study	N/A
pGB1_6xHis-GST-DmNxf3, res. 66-336	This study	JC078
Software and Algorithms		
Fiji	ImageJ	N/A
Huygens Professional Software	Scientific Volume Imaging, SVI	N/A
R	RCoreTeam	N/A
Bowtie	Langmead et al., 2009	N/A
BEDTools	Quinlan and Hall, 2010	N/A
High-throughput analysis scripts	Andersen et al., 2017	https://gitlab.com/Andersen_Moonshiner_2017

LEAD CONTACT AND MATERIALS AVAILABILITY

Further information and requests for resources and reagents should be directed to and will be fulfilled by the Lead Contact, Julius Brennecke (julius.brennecke@imba.oeaw.ac.at). *Drosophila* lines generated in this study (Table S1) are available from the Vienna stock center (https://stockcenter.vdrc.at/control/main). Additional reagents including antibodies and plasmids are available upon request.

EXPERIMENTAL MODEL AND SUBJECT DETAILS

Fly Husbandry

Flies were kept at 25°C under light/dark and humidity (60%) control. For ovary dissection, 3-5 days old flies were kept in cages with yeast supply on apple juice plates for two days and then dissected after brief immobilization by CO_2 anesthesia. A list of fly strains including genotypes, identifiers and original sources can be found in Table S1. The *w[1118]* stock served as wild type control strain throughout this work. The listed stocks are available via VDRC (http://stockcenter.vdrc.at/control/main).

Cell lines

Drosophila Schneider 2 (S2) cells (obtained from Phil Zamore; stock regularly tested to be virus- and mycoplasma-free) were grown at 25°C in S2 cell media supplemented with 10% fetal bovine serum (Thermo Fisher Scientific).

METHOD DETAILS

Generation of transgenic fly strains

We generated fly strains harboring short hairpin RNA (shRNA) expression cassettes for germline knockdown by cloning shRNA sequences into the Valium-20 vector (Ni et al., 2011) modified with a *white* selection marker (oligos are listed in Table S2). Tagged fly stains were generated via insertion of desired tag sequences into locus-containing Pacman clones via bacterial recombineering (Ejsmont et al., 2011; Venken et al., 2009). Wild-type and NES mutant Nxf3 transgenic flies were generated by inserting germline expression constructs (*nanos* promoter and *vasa* 3′ UTR) plus the corresponding coding sequences into the attP40 landing site (FlyBase ID: FBti0114379). Of note, the annotated coding sequence of Nxf3 (FlyBase ID: FBgn0263232) lacks the first 56 amino acids of the Nxf3 protein. Using CAP-seq data, we identified a transcription start site (TSS) upstream of the annotated TSS. Germline expression of the currently annotated Nxf3 tagged at the C terminus with a LAP-tag gives rise to an aberrant localization pattern. However, expression of the full ORF gives a localization pattern that is identical to the endogenously engineering locus, both of which are functional rescues. Furthermore, the non-annotated part upstream of the annotated TSS is conserved in other fly species.

Generation of mutant fly strains

Mutant alleles for *nxf3*, *CG13741*, *uap56 [E245K],* and *nxf3[D434R]* were generated through injection of pDCC6 plasmids modified to express guide-RNAs, along with ssDNA repair templates in case of point mutant generation (Gokcezade et al., 2014). Oligos and targeting sequences are given in Table S2.

Generation of endogenous knock-in fly strains

CRISPR-Cas9-mediated generation of endogenously tagged lines was through injection of pU6-BbsI-chiRNA plasmids (Addgene: 466294; Gratz et al., 2013) along with pBS donor plasmids containing 1 kb long homology arms into act-Cas9 embryos (Bloomington stock: 54590; Port et al., 2014). Oligos and targeting sequences are listed in Table S2.

Protein co-immunoprecipitation from S2 cell lysates

4 million S2 cells were transfected with 2 μg DNA using Cell Line Nucleofector kit V (Amaxa Biosystems) with the program G-030. S2 cells were co-transfected with plasmids expressing FLAG-tagged and GFP-tagged proteins driven by the actin5C promotor. After 48 hours of incubation at 25°C, S2 cells were collected through centrifugation at 600 g. The pellet was resuspended in 100 μL lysis buffer (30 mM HEPES pH 7.4, 150 mM NaCl, 2 mM $MgCl_2$, Triton X-100 0.2%), freshly supplemented with 1 mM DTT, 1 mM Pefabloc and Complete Protease Inhibitor Cocktail (Roche). Lysis was carried out at 4°C for 20 minutes followed by centrifugation for 10 minutes at 18,000 g at 4°C. Protein concentration was measured using standard Bradford assay and 500 μg of total protein were incubated with GFP-Trap magnetic beads (ChromoTek) for 3 hours at 4°C. Beads were washed 3 times 10 minutes with lysis buffer and proteins were eluted in 1x SDS loading buffer at 95°C.

Western blot analysis

Western blotting was done following standard protocols. Samples were resolved by SDS-polyacrylamide gel electrophoresis and transferred to a 0.45 μm (Bio-Rad) nitrocellulose membrane. The membrane was blocked in 5% skimmed milk powder in PBS supplemented with 0.01% Triton X-100 (PBX) for 30 minutes and incubated with primary antibody overnight at 4°C. After three washes with PBX, the membrane was incubated with HRP-conjugated secondary antibody for 2h at room temperature, followed by three washes with PBX. Subsequently, the membrane was covered with Clarity Western ECL Blotting Substrate (Bio-Rad) and imaged using the ChemiDoc MP imaging system (Bio-Rad). All relevant antibodies are listed in the Key Resources Table. For Antibody dilutions, refer to Table S4.

Antibody generation

Mouse monoclonal antibodies against His-tagged Nxf3 (amino acids T336-L614), His-tagged CG13741 (full length), and Deadlock (amino acids P470-P669) were generated by the Max Perutz Labs Antibody Facility. Nxf3 and CG13741 antigens were cloned in pET-15b and transformed in BL21(DE3) *E. coli*, and purified using Ni-NTA resin (QIAGEN) according to standard protocols. The deadlock antigen was cloned downstream of a TEV recognition site in pMAL-c2x construct to produce a maltose-binding protein (MBP)-tagged peptide, which was purified using amylose resin (NEB). The MBP-tag was cleaved by TEV protease treatment.

Recombinant protein expression and purification

Nxf3, residues 66-336, from *Drosophila melanogaster* was cloned into a modified pFastBac (Geneva Biotech) vector providing an N-terminal 6xHis-GST-tag. The resulting plasmid was transposed into the EmBacY bacmid backbone and transfected into *Spodoptera frugiperda* Sf9 cells to generate a baculovirus expressing the construct (Bieniossek et al., 2008). The virus was used to infect *Trichoplusia ni* High5 cells and expression was performed at 21°C. Cells were harvested 4 days after growth arrest. The cells were lysed in lysis buffer (LB) (50 mM Tris-HCL pH 8.0, 150 mM NaCl, 10% glycerol, 10 mM imidazole) freshly supplemented with 1 mM Pefabloc, 5 mM β-mercapto-ethanol and Benzonase (~10 U/mL) for 30 minutes at 4°C. The lysate was cleared by centrifugation. Subsequently, the protein was bound to a Ni2+-chelate affinity column (HisTrap FF 5 mL, GE Healthcare). Bound protein was eluted in LB supplemented with 250 mM imidazole and peak fractions subsequently analyzed by SDS-PAGE and Coomassie staining.

D. melanogaster $Nxf3^{488-615}$ was cloned as an N-terminal GST-fusion in pGEX-6P-1 (GE Healthcare); the M553P mutation was introduced by site directed mutagenesis. For protein expression, *E. coli* Rosetta2 (DE3) pLysS cells were grown in TB-medium at 37°C to OD_{600} ≈0.8, induced with 0.2 mM IPTG and cultured for ~16 hours at 18°C. Cells were harvested by centrifugation, resuspended in cold buffer A (50 mM Tris pH 8.0, 200 mM NaCl) supplemented with 100 μM PMSF, 1 cOmplete EDTA-free protease inhibitor cocktail tablet (Roche) per 50 mL of buffer, 10 μg/mL DNase I and 1 mg/mL lysozyme, and lysed by sonication. The lysate was cleared by centrifugation (44,000 g, 4°C, 45 min) and filtered through a 0.45 μm filter. 3 mL of Glutathione Sepharose 4B (GE Healthcare) beads were washed twice in 5 bead volumes buffer A and incubated with the lysate for 2 hours at 4°C on a rotating wheel. After removal of the supernatant and extensive washes in buffer A, the beads were incubated three times with 3 mL of freshly prepared buffer A supplemented with 10 mM reduced glutathione for 2 minutes at room temperature to elute the bound protein. The presence of GST-$Nxf3^{488-615}$ in the elutions was assessed through Coomasie-stained SDS-PAGE. Subsequently the three elutions were pooled, diluted to 100 mM NaCl, loaded on to a HiTrap Q HP 5 mL anion exchange column (GE Healthcare), and eluted in a gradient of 100 – 600 mM NaCl. Fractions containing GST-$Nxf3^{488-615}$ were again pooled, concentrated and subjected to size exclusion chromatography on a HiLoad 16/600 superdex 200 pg column (GE Helathcare), equilibrated in SEC buffer (25 mM HEPES pH 7.9, 500 mM NaCl, 5 mM $Mg(OAc)_2$, 2 mM DTT, 1 mM EDTA, 20 μM GTP). Fractions of the resulting single peak were pooled, concentrated to ~6 mg/mL, aliquoted, snap frozen in liquid N_2 and stored at −80°C.

Ran from *D. melanogaster*, residues 1-180 and carrying the Q69L mutation, was cloned into pOPIN-B (Berrow et al., 2007), which provides a N-terminal, PreScission 3C cleavable 10x His tag, and expressed as outlined for GST-$Nxf3^{488-615}$. Cells were resuspended in 50 mM K-Phosphate pH 7.0, 500 mM NaCl, 5 mM $Mg(OAc)_2$, 1 mM EDTA, 10 mM imidazole and 2 mM DTT (buffer C) supplemented with 100 μM PMSF, 1 cOmplete EDTA-free protease inhibitor cocktail tablet per 50 mL of buffer, 10 μg/mL DNase I and 1 mg/mL

lysozyme, and lysed by sonication. The lysate was treated as outlined above and loaded on a HisTrap HP 5 mL column (GE Helathcare). Protein was eluted in a 0 – 200 mM imidazole gradient in buffer C supplemented with 20 μM GTP, diluted to 150 mM NaCl and bound to a HiTrap SP HP 5 mL cation exchange column (GE Helathcare). Bound proteins were eluted in a 150 – 600 mM NaCl gradient, DmRan Q69L containing peak fractions pooled, concentrated and further purified by size exclusion chromatography as described for GST-Nxf3$^{488-615}$. DmRan Q69L was then concentrated to ~2 mg/mL and treated as described above.

Mus musculus CRM1 (full length, residues 1-1071) was expressed and purified, from an expression construct obtained from D. Görlich (Güttler et al., 2010). The 10xHis-zz-MmCRM1 protein was expressed in *E. coli* Rosetta2 (DE3) pLys cells in TB medium as outlined for GST-Nxf3$^{488-615}$. After centrifugation of the culture, cells were resuspended in 50 mM Tris/HCl pH 7.5, 500 mM NaCl, 1 mM EDTA, 10 mM imidazole (buffer D) supplemented with 100 μM PMSF, 1 cOmplete EDTA-free protease inhibitor cocktail tablet per 50 mL of buffer, 10 μg/mL DNase I and 1 mg/mL lysozyme; following sonication and centrifugation, the cleared lysate was load on a HisTrap HP 5 mL column (GE Healthcare). After an additional wash step with buffer D supplemented with 100 mM KCl, 10 mM $Mg(OAc)_2$ and 1 mM ATP, bound protein was eluted in a 0 – 200 mM imidazole gradient in buffer D. MmCRM1-containing fractions were diluted to 100 mM NaCl and further purified by anion exchange and size exclusion chromatography as described for GST-Nxf3$^{488-615}$. Purified MmCRM1 was concentrated to 8 mg/mL, aliquoted and frozen as outlined above.

Protein concentrations were calculated using their molar extinction coefficient and the theoretical molecular weight for GST-Nxf3$^{488-615}$ (41.1 kDa), 6xHis-3C-DmRan$^{1-180}$ Q69L (22.9 kDa) and 10xHis-zz-3C-MmCRM1 (139.2 kDa).

Pulldown experiments

For each pulldown 20 μL Glutathione Sepharose 4B (GE Healthcare) beads were washed twice with 20 bead volumes of PD buffer (25 mM HEPES pH 7.9, 150 mM NaCl, 5 mM $Mg(OAc)_2$, 2 mM DTT, 1 mM EDTA, 20 μM GTP). 10 μg of GST-Nxf3$^{488-615}$ or GST-Nxf3$^{488-615}$ carrying the M553P mutation was mixed with a 5-fold molar excess of MmCRM1 (170 μg) in the presence or absence of 5-fold molar excess DmRan$^{1-180}$ Q69L (28 μg). To rule out unspecific binding of MmCRM1 and DmRan to the beads, one reaction was carried out without GST-tagged bait protein. All mixtures were adjusted to a final volume of 35 μL. To reduce the salt concentration to 150 mM NaCl, samples were diluted 3.3-fold by dropwise addition of PD buffer without salt. After a pre-incubation of 15 minutes on ice, 20 μL of pre-equilibrated beads were added to each pulldown and the reactions incubated on a rotating wheel for 30 minutes at room temperature. After the supernatant was removed, the beads were washed 5 times with 200 μL of PD buffer. Subsequently, the beads were incubated 2 minutes at room temperature in 40 μL of freshly prepared PD buffer supplemented with 10 mM reduced Glutathione to elute bound proteins. Bound proteins and input samples of the individual recombinant proteins were separated on 4 – 12% gradient SDS-PAGE gels and visualized through Coomassie staining.

Electrophoretic mobility shift assay (EMSA)

2.5 nmol [32P] 5′-labeled single stranded 35 nt RNA (CUCAUCUUGGUCGUACGC GGAAUAGUUUAAACUGU) was equilibrated with various concentrations of recombinant 6xHis-GST-Nxf3 (66-336) or GST in 10 μL total volume in EMSA binding buffer (10 mM Tris-HCL pH = 8.5, 1 mM EDTA, 100 mM KCl, 5% glycerol), freshly supplemented with RNase inhibitor, 1 mM DTT and BSA (10 μg/mL). The reactions were incubated at 4°C for 20 minutes. 2 μL of EMSA loading buffer (50% glycerol, 0.075% bromophenol blue) was added and the total reaction volumes were analyzed on a pre-run 4.8% PAGE gel in 0.5 x TBE. The radioactive bands were visualized with an Amersham Typhoon Imaging System (GE Healthcare).

Protein co-immunoprecipitation from ovary lysates

Ovary samples (100 to 200 ovary pairs) were dissected and transferred to ice-cold PBS. After PBS removal, ovaries were then snap-frozen for later processing. For immunoprecipitation, ovary samples were homogenized with 20-30 strokes of a glass douncer with a tight pestle in 1 mL Ovary Protein Lysis Buffer (20 mM Tris-HCl pH 7.5, 150 mM NaCl, 2 mM $MgCl_2$, 10% glycerol, 1 mM DTT, 1 mM PefaBloc, 0.2% NP-40). Homogenates were transferred to 1.5 mL low-retention tubes and incubated on ice for 15 minutes with occasional inversion. The lysates were cleared by centrifugation for 5 minutes at 16.000*g*. Cleared lysates were added to 20 μL anti-FLAG M2 magnetic bead (Sigma) solution (50% beads per total volume with Beads Buffer (20 mM Tris-HCl pH 7.5, 150 mM NaCl)). Lysate-bead mixtures were incubated 3 hours at 4°C with rotation and then washed four times 10 minutes in Ovary Protein Lysis Buffer followed by six quick rinses in Co-IP Wash Buffer (20 mM HEPES pH 7.4, 150 mM NaCl, 2 mM $MgCl_2$). Pelleted magnetic beads were stored at 4°C in 10 μL Co-IP Wash Buffer until processing for mass spectrometry analysis the following day.

Mass Spectrometry Analyses

Co-immuno-precipitated proteins were subjected to on-bead digestion with LysC. The hereby eluted peptides were digested with Trypsin overnight. The resulting peptides were analyzed using a Dionex UltiMate 3000 HPLC RSLC nano system coupled to a Q Exactive mass spectrometer equipped with a Proxeon nanospray source (Thermo Fisher Scientific). Peptides were eluted using a flow rate of 230 nL min^{-1}, and a binary 3 hour gradient, respectively 225 minutes and the data were acquired with the mass spectrometer operated in data-dependent mode with MS/MS scans of the 10 most abundant ions. For peptide identification, the RAW-files were loaded into Proteome Discoverer (version 2.1.0.81, Thermo Scientific) and the created MS/MS spectra were searched using MSAmanda v1.0.0.6186 (Dorfer et al., 2014) against *Drosophila melanogaster* reference translations retrieved from Flybase

(dmel_all-translation-r6.17). An in-house-developed tool apQuant (Doblmann et al., 2018) was used for the peptide and protein quantification (IMP/IMBA/GMI Protein Chemistry Facility; http://ms.imp.ac.at/index.php?action=apQuant). Average enrichment between bait and control IP experiments were plotted against p values calculated using the limma R package (Smyth, 2004).

Yeast Two-Hybrid Analysis

Yeast two-hybrid screening was performed by Hybrigenics Services, S.A.S., Paris, France (https://www.hybrigenics-services.com). The coding sequence for full-length *Drosophila melanogaster* deadlock (NCBI: NM_136247.3) was PCR-amplified and cloned into pB27 as a C-terminal fusion to LexA (LexA-del). The construct was sequence verified and used as a bait to screen a random-primed *Drosophila* ovary cDNA library constructed into pP6. pB27 and pP6 derive from the original pBTM116 (Vojtek and Hollenberg, 1995) and pGADGH (Bartel et al., 1993) plasmids, respectively. 105 million clones (10-fold the complexity of the library) were screened using a mating approach with YHGX13 (Y187 ade2-101::loxP-kanMX-loxP, matα) and L40ΔGal4 (mata) yeast strains as previously described (Fromont-Racine et al., 1997). 185 His+ colonies were selected on a medium lacking tryptophan, leucine and histidine, and supplemented with 1 mM 3-aminotriazole to handle bait auto-activation. The prey fragments of the positive clones were amplified by PCR and sequenced at their 5′ and 3′ junctions. The resulting sequences were used to identify the corresponding interacting proteins in the GenBank database (NCBI).

In order to validate screen hits, yeast two hybrid experiments were carried out as described in Miller and Stagljar (2004). Briefly, proteins of interest were fused either to binding domain (BD) or the activation domain (AD) of the Gal4 transcription factor and transformed into PJ694A (AD) and PJ694α (BD). Transformed haploid cells were mated according to standard yeast protocols. Interaction of the fusion proteins will lead to the reconstitution of the Gal4 transcription factor and activation of the ADE2 and HIS3 reporter genes. Reporter genes activation can readout as growth on the respective selective medium. Yeast strains used in this study are listed in the Table S3.

RT-qPCR analysis of transposon expression

Five pairs of dissected ovaries were homogenized in TRIzol reagent followed by RNA purification according to the manufacturer's protocol. 1 μg of total RNA was digested with RQ1 RNase-free DNase (Promega) and then reverse transcribed using anchored oligo dT primers and Superscript II (Invitrogen) following standard protocols. cDNA was used as template for RT-qPCR quantification of transposon mRNA abundances (for primer sequences see Table S2).

Immuno-gold Electron Microscopy

Freshly dissected ovaries were fixed in 2% paraformaldehyde and 0.2% glutaraldehyde (both EM-grade, EMS, USA) in 0.1 M PHEM buffer (pH 7) for 2 hours at room temperature, then overnight at 4°C. The fixed ovaries were embedded in 12% gelatin and cut into 1 mm^3 blocks which were immersed in 2.3 M sucrose overnight at 4°C. These blocks were mounted onto Leica specimen carrier (Leica Microsystems, Austria) and frozen in liquid nitrogen. With a Leica UCT/FCS cryo-ultra-microtome (Leica Microsystems, Austria) the frozen blocks were cut into ultra-thin sections at a nominal thickness of 60 nm at −120°C. A mixture of 2% methylcellulose (25 centipoises) and 2.3 M sucrose in a ratio of 1:1 was used as a pick-up solution. Sections were picked up onto 200 mesh Ni grids (Gilder Grids, UK) with a carbon coated formvar film (Agar Scientific, UK). Fixation, embedding and cryo-sectioning as described by Tokuyasu (1973). Prior to immuno-labeling, grids were placed on plates with solidified 2% gelatin and warmed up to 37°C for 20 minutes to remove the pick-up solution. After quenching of free aldehyde-groups with glycin (0.1% for 15 minutes), a blocking step with 1% BSA (fraction V) in 0.1 M Sörensen phosphate buffer (pH 7.4) was performed for 30 minutes. The grids were incubated in primary antibody (rabbit polyclonal against GFP; ab6556, Abcam, UK), diluted 1:125 in 0.1 M Sörensen phosphate buffer over night at 4°C, followed by a 2 hour incubation in the secondary antibody (goat-anti-rabbit antibody coupled with 6 nm gold; GAR 6 nm, Aurion, the Netherlands), diluted 1:20 in 0.1 M Sörensen phosphate buffer, performed at RT. The sections were stained with 4% uranyl acetate (Merck, Germany) and 2% methylcellulose in a ratio of 1:9 (on ice). All labeling steps were done in a wet chamber. The sections were inspected using a FEI Morgagni 268D TEM (FEI, the Netherlands) operated at 80kV. Electron micrographs were acquired using an 11 megapixel Morada CCD camera from Olympus-SIS (Germany).

Immunofluorescence staining of ovaries

5-10 ovary pairs were dissected into ice-cold PBS and subsequently fixed by incubation for 20 minutes at room temperature in IF Fixing Buffer (4% formaldehyde, 0.3% Triton X-100, 1x PBS) with rotation. Fixed ovaries were washed three times 10 minutes in PBX (0.3% Triton X-100, 1x PBS) and blocked with BBX (0.1% BSA, 0.3% Triton X-100, 1x PBS) for 30 minutes, all at room temperature with rotation. Primary antibody incubation was performed by overnight incubation at 4°C with antibodies diluted in BBX followed by three 10 minute-washes in PBX. Ovaries were then incubated overnight at 4°C with fluorophore-coupled secondary antibodies, washed once in PBX, incubated with wheat germ agglutinin (WGA)-coupled Alexa Fluor 488 (Thermo Fisher Scientific) at a 1:200 dilution in PBX for 20 minutes, and washed three times in PBX with the second wash done with DAPI added to the PBX to stain DNA (1:50.000 dilution). The final wash buffer was carefully removed, and each sample was resuspended in ~40 μL Prolong Diamond mounting medium and 10 μL of 0.5μm TetraSpeck beads (Thermo Fisher Scientific). The samples were imaged on a Zeiss LSM-880 Axio Imager confocal-microscope and the resulting images processed using FIJI/ImageJ (Schindelin et al., 2012). TetraSpeck beads were imaged separately in a Z stack of 320 nm. Dotted lines representing nuclear envelope position were drawn

in the represented images based on WGA or DAPI signal as indicated in the figure legends. All relevant antibodies are listed in the Key Resources Table. For Antibody dilutions, refer to Table S4.

Immunofluorescence staining of S2 cells

24 hours after transfection, 30,000 cells were seeded onto removable chambered cover glass (Grace Bio-Labs), freshly coated with Concanavalin A, for 3 hours. Cells were washed with PBS for 5 minutes and subsequently fixed with formaldehyde solution (4% formaldehyde in PBS) for 20 minutes at room temperature. If indicated, cells were treated with 20 ng/mL Leptomycin B (LMB, Sigma Aldrich) prior to fixation. Fixed cells were washed twice with PBS for 5 minutes, permeabilized with 0.3% Triton X-100 in PBS for 10 minutes and washed again with PBS for 5 minutes. Blocking was done in BBX (PBX (0.01% Triton X-100 in PBS) + 1% BSA) for 20 minutes. Cells were incubated with primary antibody in BBX at 4°C overnight. Following three washing steps with PBX, cells were incubated with fluorophore-conjugated secondary antibody in BBX for 2 hours at room temperature in the dark. Stained cells were washed three times with PBX. Where indicated, the cells were incubated in wash buffer containing wheat germ agglutinin (WGA)-coupled Alexa Fluor 647 conjugate at a final concentration of 5 ng/μL and then incubated for 15 minutes at room temperature with agitation. Otherwise, DAPI stain (1: 5000) was included in the second wash. The coverslip was removed from culture chambers and each sample was mounted using one drop of ProLong Diamond Antifade Mountant (Thermo Fisher Scientific). Mounted samples were imaged with a Zeiss LSM-880 confocal microscope and the images were processed using FIJI/ImageJ. Dotted lines representing nuclear envelope position were drawn in the represented images based on WGA or DAPI signal as indicated in the figure legends.

RNA Fluorescent *In Situ* Hybridization (FISH)

Freshly dissected ovary pairs (5-10 for each sample) were fixed in formaldehyde solution (4% formaldehyde, 0.15% Triton X-100 in PBS) for 20 minutes at room temperature, washed three times for 10 minutes in 0.3% Triton X-100/PBS, and permeabilized overnight in 70% ethanol at 4°C. Permeabilized ovaries were rehydrated for 5 minutes in RNA FISH wash buffer (10% (v/w) formamide in 2 × SSC). Ovaries were resuspended in 50 μL hybridization buffer (10% (v/w) dextran sulfate and 10% (v/w) formamide in 2 × SSC) containing 0.5 μL of each RNA FISH probe set solution (see Table S2 for probe sequences and below for probe source) and hybridized overnight at 37°C with rotation. Next, ovaries were rinsed twice in RNA FISH wash buffer, resuspended in RNA FISH wash buffer containing wheat germ agglutinin (WGA)-coupled Alexa Fluor 488 or 647 conjugate at a final concentration of 5 ng/μL and then incubated for 1h at room temperature with agitation. Ovaries were then subjected to four washes: once for 30 minutes at room temperature in RNA FISH wash buffer, once for 10 minutes in a DAPI/2xSSC solution and finally twice for 10 minutes in 2 × SSC buffer. The final wash buffer was carefully removed, and each sample was resuspended in ~40 μL Prolong Diamond mounting medium and 10 μL of 0.5μm TetraSpeck beads (Thermo Fisher Scientific), and mounted on a microscopy slide. The mounted samples were allowed to equilibrate for at least 24 hours before imaging on a Zeiss LSM 880 confocal microscope equipped with an AiryScan detector. Ovary germline nuclei from stage 6-9 egg chambers were imaged separately with a × 63 oil lens in a *Z*-stack of 120 planes of 150 nm intervals. TetraSpeck beads were imaged separately in a Z stack of 320 nm. All probe sets were generated as custom Stellaris RNA FISH probe sets (Biosearch Technologies; dissolved to 25 μM) except the *cluster80F* probe set which was generated by terminal oligonucleotide labeling using Atto-565 according to Gaspar et al. (2017).

Imaging data analysis for localization studies

Imaging data analysis was done as described in Andersen et al. (2017) with modifications. Specifically, acquired images were deconvolved using Huygens Professional Software (Scientific Volume Imaging, SVI). Chromatic aberrations in every sample were measured using TetraSpeck beads and corrected using Chromatic Aberration Correction (CAC) macro which relied on the Descriptor-based registration plugin (Preibisch et al., 2010). The deconvolved and beads-aligned images were segmented using the DAPI and WGA signals into nuclear and nuage regions. Channel 1 (*cluster20A* RNA FISH in far-red channel) and Channel 2 (*cluster42AB* RNA FISH in the red channel) in case of null mutant experiments and Channel 1 (*cluster42AB* RNA FISH in the red channel) and Channel 2 (GFP-tagged protein in the green channel) in case of protein localization experiments. For segmentation, a Difference-of-Gaussian (DoG) filter was applied to the channels before thresholding. The center pixels of the loci were determined by finding local maxima using a Min/Max filter. These centers were then used as seed points for splitting compound objects as well as to calculate the distance of each focus to the prior defined nuclear envelope. Size and intensity thresholds were applied to exclude ambiguous objects. Intensities, size, number, and distances per identified foci, cell and channel was exported for analysis and plotting in R. Dotted lines representing nuclear envelope position were drawn in the represented images based on WGA signal.

Defining and Curating 1 kb Genomic Windows

The *Drosophila melanogaster* genome (dm6 assembly) was split into non-overlapping 1-kb tiles. The tiles were annotated by intersection with gene and piRNA cluster genomic annotations. Tile mappability scores – an estimate of the amount of unique sequence space per tile – were calculated by mapping 25 bp synthetic genome-derived reads back to the genome and calculating the number of uniquely mapping reads per tile. Tile annotation and curation can be reproduced using the scripts available through Andersen et al. (2017).

ChIP-Seq library preparation

Chromatin immunoprecipitation (ChIP) was performed as previously described (Lee et al., 2006) with minor modifications. Briefly, 100 ovary pairs were dissected into ice-cold PBS and cross-linked in 1.8% para-formaldehyde/PBS for 10 minutes at room temperature with agitation. The cross-linking reaction was quenched by addition of glycine and ovaries were washed in PBS and homogenized in a glass douncer with a tight pestle. The homogenates were then lysed on ice for 20 minutes. DNA was sheared using a Covaris E220 Ultrasonicator, sonicating each sample for 20 minutes at 4°C with 200 cycles per burst, duty factor at 5.0 and peak incident power (PIP) set to 140 W. The sonicated lysates were cleared by centrifugation and then incubated overnight at 4°C with antibodies specific to the target epitope. 50 μL 1:1 mix of Protein A and Protein G Dynabeads was then added and allowed to bind antibody complexes by incubation for 2 hours at 4°C. Following six washing steps, DNA-protein complexes were eluted and de-cross-linked overnight at 65°C. RNA and protein was digested by RNase A and Proteinase K treatment, respectively, before purification using ChIP DNA Clean & Concentrator columns (Zymo Research). Barcoded libraries were prepared using the NEBNext Ultra II DNA Library Prep Kit for Illumina (NEB), which were sequenced on a HiSeq2500 (Illumina).

ChIP-Seq Analysis

ChIPseq reads were trimmed to high quality bases 5-45 before mapping to the *Drosophila melanogaster* genome (dm6, r6.18) using Bowtie (release 1.2.2) (Langmead et al., 2009) with 3-mismatch tolerance. Reads were then computationally extended to the library median insert length of 353 nt. Normalization between samples was done based on the number of genome-unique mapping reads for each sample. Subsequent quantification of reads mapping to 1-kb tiles was done using bedtools (Quinlan and Hall, 2010), while relative quantification and plotting was done in R (see Quantification and Statistical Analyses below). Briefly, Rhino ChIP-seq tile signal was normalized to corresponding values for the relevant ChIP input libraries. A pseudo-count of 1 was then added to each tile value before calculation of log2 fold-enrichment values relative to input.

RNA-Seq library preparation

For RNaseq libraries from samples depleted of rRNA by RNaseH-treatment (RH RNaseq), we modified the protocol published in Morlan et al. (2012). TRIzol-isolated total RNA was purified by RNAeasy columns with on-column DNase I digest (QIAGEN) in accordance with manufacturer's instructions. Depletion of rRNA from the purified total RNA was done by using a mix of antisense oligonucleotides matching *Drosophila melanogaster* rRNAs (listed in Table S2). The oligonucleotides were added to the 1 μg RNA in RNase H Buffer (20 mM Tris-HCl pH = 8, 100 mM NaCl) and annealed with a temperature gradient from 95°C to 45°C. The RNA-DNA hybrids were specifically digested with Hybridase Thermostable RNase H (Epicenter) at 45°C for 1 hour. Next, DNA was digested with TURBO DNase (Invitrogen) and RNA was purified using RNA Clean & Concentrator-5 (Zymo) according to the manufacturer's instructions. Libraries were then cloned using the NEBNext Ultra II Directional RNA Library Prep Kit for Illumina (NEB), following the recommended kit protocol and sequenced on a HiSeq2500 (Illumina).

PolyA-enriched RNaseq libraries were prepared in an automated setup on a Biomek i7 robot. Briefly, 0.5 μg total RNA was denatured at 72°C for 3 minutes, then put on ice. PolyA+ enrichment was done with the NEBNext Poly(A) mRNA Magnetic Isolation Module (NEB) according to the manufacturer's recommendations. DNA was prepared from polyA+ RNA using NEB Ultra II Directional First and Second Strand Synthesis modules (NEB) according to the manufacturer's recommendations, but incubating only 7 minutes at 94°C. The cDNA was purified with 1.5x AmpureXP beads and subjected to NEB Ultra II DNA library preparation Kit. PCR fragments of 200-800 bp were purified and sequenced on a NextSeq550 instrument (Illumina).

RNA-Seq Analysis

RNA-Seq reads were trimmed to high quality bases 5-45 before mapping to the *Drosophila* genome (dm6, r6.18) using STAR (Dobin et al., 2013) or to *Drosophila melanogaster* mRNA and transposon and host mRNA sequences using Salmon (0.10.2) (Patro et al., 2017). For genomic mapping by STAR, normalization between samples was done based on the number of genome-unique mapping reads for each sample. Subsequent quantification of reads mapping to 1-kb tiles (performed for RH RNaseq only) was done using bedtools (Quinlan and Hall, 2010), while relative quantification and plotting was done in R (see Quantification and Statistical Analyses below). Briefly, RNA-seq tile signal was normalized to the estimated mappability scores for each 1 kb window. A pseudo-count of 1 was then added to each tile value before calculation of log2 fold-change values relative to control genotype samples. For analyses of transposon and host mRNA levels, only poly-A-enriched RNaseq libraries were used in order to avoid confounding the analyses with non-polyadenylated piRNA precursor transcripts. For each library, transcripts-per-million-transcripts (TPM) values were calculated using Salmon (0.10.2). TPMs were inter-sample-normalized using Sleuth (0.30.0) (Pimentel et al., 2017).

Small RNA-Seq library preparation

Small RNA libraries were generated as described by Jayaprakash et al. (2011) with modifications. Briefly, 18-29 nt long small RNAs were purified by preparative PAGE from 10 μg of total ovarian RNA. Following, the 3′ linker (containing four random nucleotides) was ligated overnight using T4 RNA Ligase 2, truncated K227Q (NEB) after which the products were recovered by a second PAGE purification. 5′ RNA linkers with four terminal random nucleotides were then ligated to the small RNAs using T4 RNA ligase (NEB)

followed by an SPRI magnetic bead purification (in-house-produced beads similar to Agencourt RNAclean XP). The cloned small RNAs were then reverse transcribed and PCR amplified before sequencing on a HiSeq2500 (Illumina). Cloning oligo sequences are given in Table S2.

Small RNA-Seq Analysis

Single-end, 50-nucleotide small RNA sequencing reads were trimmed by removal of the 3′ linker sequence (AGATCGGAAGAGCACACGTCT), as well as the four random nucleotides at each end. Trimmed reads were mapped to the *Drosophila* genome (dm6, r6.18) using Bowtie (release 1.2.2) (Langmead et al., 2009) with 0-mismatch tolerance. Genome coverage was calculated and normalized to the number of uniquely mapping microRNA reads (in millions). Reads mapping to rRNA, tRNA, snRNA and snoRNA were excluded. Subsequent quantification of reads mapping to 1-kb tiles was done using bedtools (Quinlan and Hall, 2010), while relative quantification and plotting was done in R (see Quantification and Statistical Analyses below). Briefly, small RNA-seq tile signal was normalized to the estimated mappability scores for each 1 kb window. A pseudo-count of 1 was then added to each tile value before calculation of log2 fold-change values relative to control genotype samples.

RIP-Seq library preparation

RIPseq protocol was adapted from Zhang et al. (2012) with modifications. 80-100 ovaries from well fed flies (3-5 days old) were dissected in ice-cold PBS and homogenized by 20 pestle strokes in RIP lysis buffer (50mM HEPES pH 7.3, 150mM KCL, 3.2 mM MgCl, 0.5% TERGITOL solution (Sigma)) freshly supplemented with RNaseOUT (2.5μL/mL), 1mM Pefabloc, cOmplete Protease Inhibitor Cocktail (Roche), and 0.5 mM DTT. The lysate was sonicated using Bioruptor at medium strength (15 s ON, 60 s OFF), and cleared by centrifugation at 14,000 rpm for 15 minutes at 4°C. 5% of cleared lysate were set aside to serve as input samples, while the remainder was incubated at 4°C with 30 μL anti-FLAG M2 magnetic beads for 3 hours. The beads were washed 2 times with RIP lysis buffer for 10 minutes, transferred into a fresh tube, and washed for 2 more times with all washes performed at 4°C. RNA was extracted from input lysate and beads using TRIzol reagent (Invitrogen) according to manufacturer's instructions, further purified using the RNA Clean & Concentrator-5 kit (Zymo Research) with In-Column DNase I treatment, and eluted in 8 μL nuclease free water. Half of the eluted RNA was used for strand-specific RIP-Seq library preparation using the NEBNext Ultra II Directional RNA Library Prep Kit (New England Biolabs).

RIP-qPCR

Enrichment of cluster transcripts after RIP was assayed by RT-qPCR. cDNA was synthesized from 2 μL of purified and DNase treated RIP-RNA using the Maxima First Strand cDNA Synthesis Kit (Thermo Fisher Scientific) according to manufacturer's protocol. cDNAs were amplified using primers listed in Table S2. qPCR reactions were performed using GoTaq qPCR system (Promega).

RIP-Seq analyses

RIP-Seq reads were trimmed to high quality bases 5-45 before mapping to the *Drosophila* genome (dm6, r6.18) using STAR (Dobin et al., 2013). Normalization between samples was done based on the number of high-quality reads sequenced for each sample. Subsequent quantification of reads mapping to 1-kb tiles was done using bedtools (Quinlan and Hall, 2010), while relative quantification and plotting was done in R (see Quantification and Statistical Analyses below). Briefly, RIP-seq tile signal was normalized to corresponding values for the relevant RIP input libraries. A pseudo-count of 1 was then added to each tile value before calculation of log2 fold-enrichment values relative to control RIP libraries from immunoprecipitation of NLS-GFP-V5-3xFLAG fusion proteins expressed in ovary nurse cells.

PRO-Seq library preparation

PRO-seq was performed as described previously (Mahat et al., 2016), with modifications. Briefly, for each genotype, 50 μL ovaries were dissected into ice-cold PBS. Ovaries were then fragmented by douncing using a tight glass pestle and the homogenates were permeabilized and crude nuclei fractions were prepared by washing in permeabilization buffer. The permeabilized ovary samples were then stored at −80°C in *storage buffer* until further processing. Nuclear run-on reactions were performed with biotin-11-CTP and biotin-11-UTP and unlabeled ATP and GTP. Following RNA purification from the run-on reactions, RNA samples were fragmented for 10 minutes on ice in 0.2 N NaOH and purified on Bio-Spin P30 columns (Bio-Rad). Biotin-labeled RNA was then purified using MyOne Streptavidin C1 Dynabeads (Thermo Fisher Scientific) and decapped using Tobacco Acid Pyrophosphatase (TAP) enzyme (Epicenter, can be replaced by RppH from NEB) and purified by phenol/chloroform extraction. 3′ linkers and then 5′ linkers (same as for small RNA cloning) were then ligated subsequently and biotinylated ligation products were purified after each ligation using MyOne Streptavidin C1 Dynabeads. Reverse transcription was performed using SuperScript II enzyme (Thermo Fisher Scientific) and the cloned libraries were PCR amplified using KAPA Hotstart Realtime master mix (KAPA Biosystems). The amplified libraries were then sequenced on a HiSeq2500 (Illumina) in paired-end 75 bp mode.

PRO-Seq analysis

Second mate-pair reads, representing RNA 3′ ends, were mapped to the *Drosophila* genome (dm6, r6.18) using STAR (Dobin et al., 2013). Normalization between samples was done based on the number of genome-unique mapping reads for each sample. Subsequent quantification of reads mapping to 1-kb tiles was done using bedtools (Quinlan and Hall, 2010), while relative quantification and plotting was done in R (see Quantification and Statistical Analyses below). Briefly, PRO-Seq tile signal was normalized to the estimated mappability scores for each 1 kb window. A pseudo-count of 1 was then added to each tile value before calculation of log2 fold-change values relative to control genotype samples.

NXF family protein sequence alignments

Sets of sequences orthologous to *D. melanogaster* Sbr (Nxf1) and Nxf3 were collected using reciprocal protein blast searches. A multiple sequence alignment of the selected sequences was generated using mafft (v7.407) and visualized using Jalview (v2.10.2b2) with the Clustal color-scheme. All sequence accession numbers are given in Table S5.

DATA AND CODE AVAILABILITY

All sequencing data produced for this publication has been deposited to the NCBI GEO archive under the accession number GSE126578.

The mass spectrometry proteomics data have been deposited to the ProteomeXchange Consortium via the PRIDE (Vizcaíno et al., 2016) partner repository with the dataset identifier PRIDE: PXD012717.

High-throughput sequencing analysis scripts were directly adapted (see above sections for the specific mapping and normalization settings for each sequencing method) from the scripts published in Andersen et al. (2017). These scripts are available at https://gitlab.com/Andersen_Moonshiner_2017.

QUANTIFICATION AND STATISTICAL ANALYSES

Data visualization and statistical analyses were done using R (RCoreTeam, 2018) in conjunction with the following software packages: ggplot2 (Wickham, 2016), tidyverse (https://www.tidyverse.org/) and scales (Wickham, 2017). The UCSC genome browser (Kent et al., 2002; Raney et al., 2013) was used to explore sequencing data and to prepare genome browser panels shown in the manuscript. Boxplots (such as Figure 2B) display median (line), first and third quartiles (box), and highest/lowest value within 1.5 × interquartile range (whiskers). A Mann–Whitney–Wilcoxon statistical test was performed on the quantitative RNA FISH data shown in Figure 2J to determine if the tested sample populations have similar distributions.

ADDITIONAL RESOURCES

Genome browser session: http://genome-euro.ucsc.edu/s/Refsing/Nxf3_public_session

Interactive MS plots: http://brenneckelab.imba.oeaw.ac.at/tmp/nxf3_paper/MS_plots/

Supplemental Figures

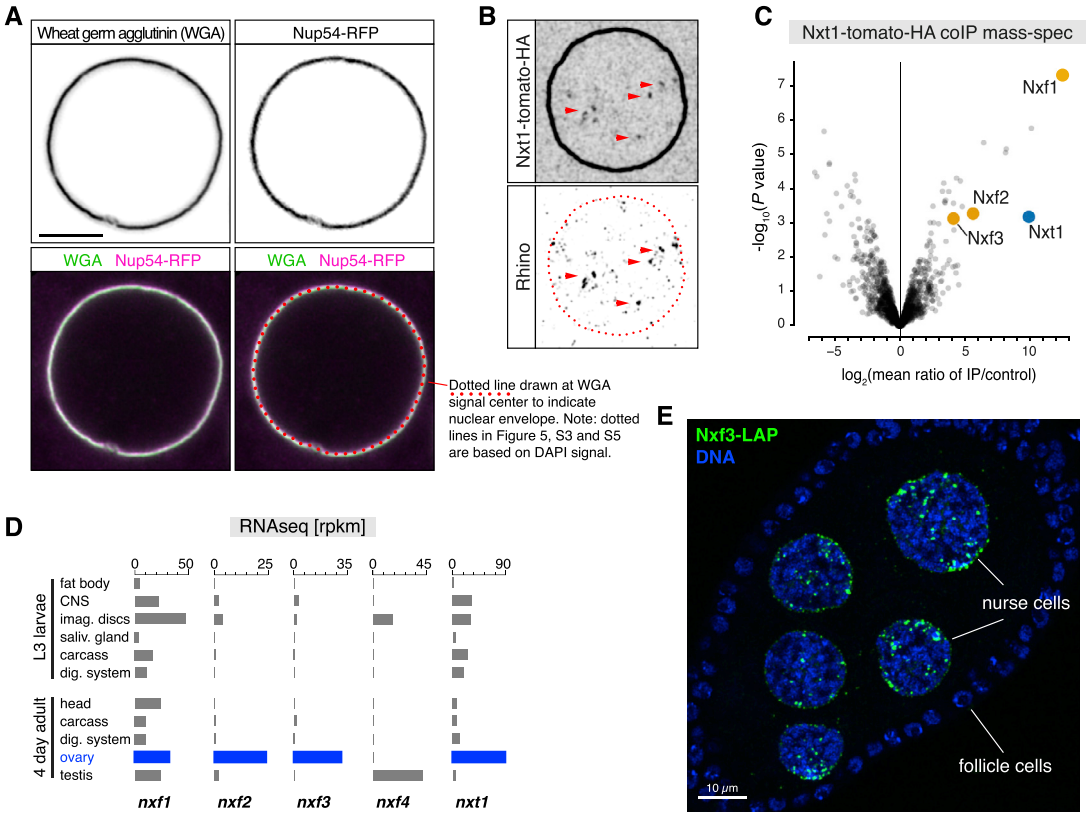

(legend on next page)

Figure S1. Related to Figure 1

(A) Confocal images of a nurse cell nucleus (~stage 8 egg chamber; scale bar: 5 μm) expressing Nup54-RFP under its endogenous promoter region, stained for nuclear pore complexes with wheat germ agglutinin (WGA). The WGA signal overlaps precisely with that of Nup54-RFP. Throughout the paper, we used WGA to visualize the nuclear envelope (red dotted line corresponds to center of WGA signal; lower right panel).

(B) Localization of Nxt1-tdTomato-HA alongside Rhino in nurse cells (red dotted line: nuclear envelope; red arrowheads: Rhino foci; scale bar: 5 μm).

(C) Volcano plot showing enrichment values and corresponding significance levels for proteins co-purifying with Nxt1-tdTomato-HA from ovaries versus control (Wild-type ovaries; n = 3).

(D) mRNA levels as determined by RNaseq for indicated genes from indicated larval or adult tissues (data from FlyBase (Brown et al., 2014)).

(E) Confocal image of an entire egg chamber expressing Nxf3-LAP from its endogenous locus (nurse cell and follicle cell nuclei are indicated; scale bar: 10 μm).

(F–G) Transmission electron microscopy images of nurse cells at different magnifications. The nuclear envelope is pseudo-colored (blue), also indicated are mitochondria, nuage (electron-dense perinuclear structures), nucleus and cytoplasm. Sections were stained with a polyclonal anti-GFP antibody and a secondary anti-rabbit antibody coupled to 6 nm gold particles ((F) ovaries expressing Vasa-GFP; (G) ovaries expressing Nxf3-GFP).

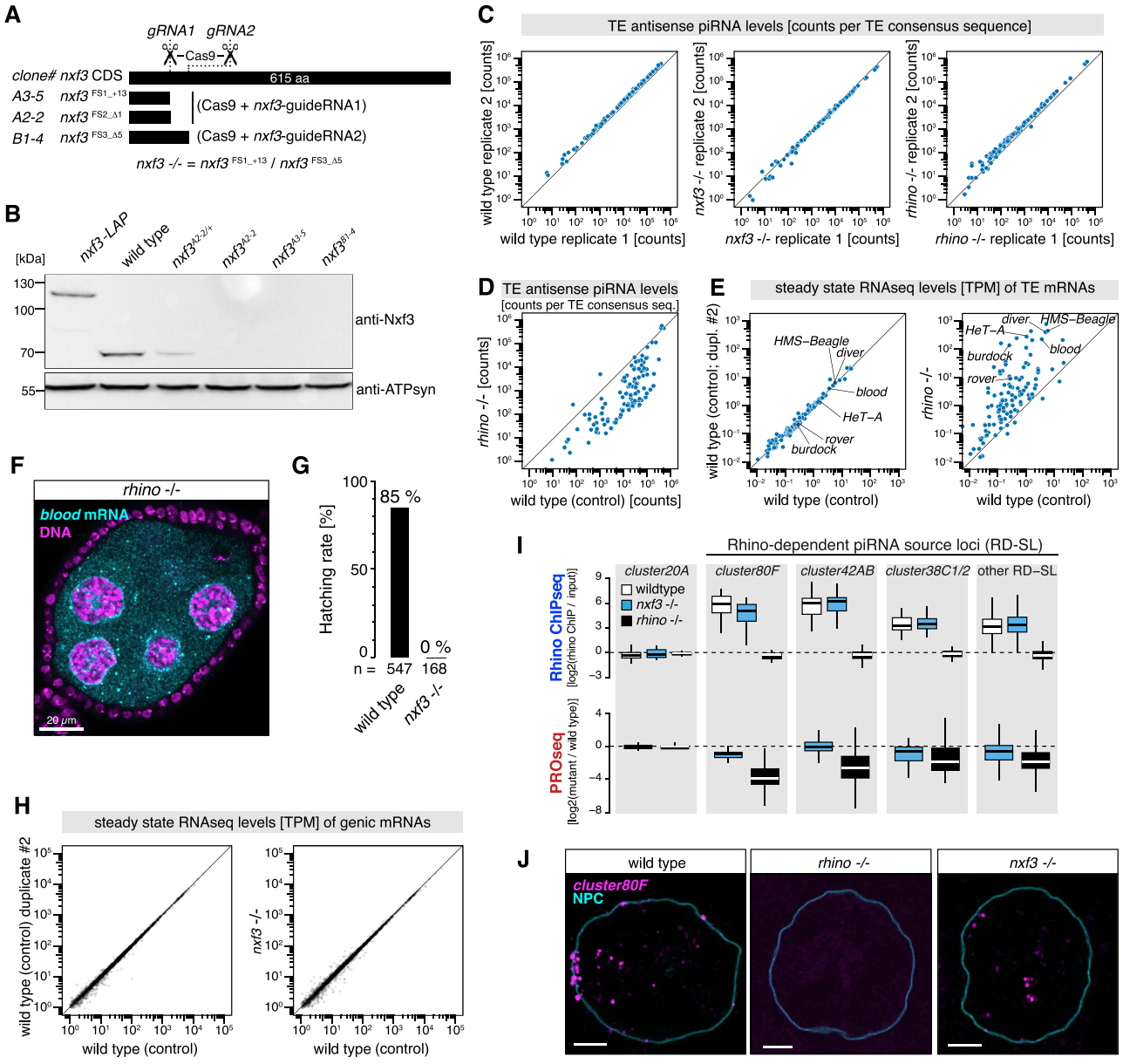

Figure S2. Related to Figure 2

(A) Cartoon depicting the frameshift mutations in *nxf3* generated by CRISPR/Cas9 using two independent single guide RNAs. The allelic null allele combination used throughout this paper is indicated at the bottom.

(B) western blot analysis using a monoclonal antibody raised against Nxf3 verifying the endogenous LAP-tagging at the *nxf3* locus (lane 1), and the *nxf3* mutant frameshift alleles (lanes 4-6). A staining against ATP-synthase serves as loading control.

(C) Scatterplots displaying levels of antisense piRNAs mapping to consensus transposon sequences from ovary samples of the two replicates per genotype.

(D) Scatterplot displaying levels of antisense piRNAs mapping to consensus transposon sequences from control ovary samples versus *rhino* mutant samples.

(E) Scatterplots displaying levels of sense RNA reads mapping to consensus transposon sequences from ovary samples of indicated genotype.

(F) Confocal image of *rhino* mutant egg chamber showing the *blood* transposon mRNA (FISH: cyan; DAPI: magenta). Image taken under identical settings as those shown in Figure 2F.

(G) Bar plot indicating embryo hatching rate of eggs laid by wildtype (*w[1118]*) control females and *nxf3* mutant females.

(H) Scatterplots displaying steady state mRNA levels (transcripts per million transcripts, TPM) from ovary samples of indicated genotype.

(I) Boxplot displaying log2 fold changes in Rhino occupancy (top panel; ChIP-seq) or transcriptional output (bottom panel; PRO-seq) at indicated genomic loci in ovaries of indicated genotypes. Contrasted is the Rhino-independent piRNA *cluster20A* against Rhino-dependent piRNA clusters (*42AB*, *80F*, *38C1+2*, others). Individual data points underlying the boxes are genomic 1-kb tiles, only reads mapping uniquely to each locus were considered. Boxplot definition as in Figure 2B.

(J) Confocal images (scale bar: 5 μm) of nurse cell nuclei (genotypes indicated) stained with RNA-FISH for *cluster80F* transcripts (magenta) alongside nuclear pores (WGA: cyan).

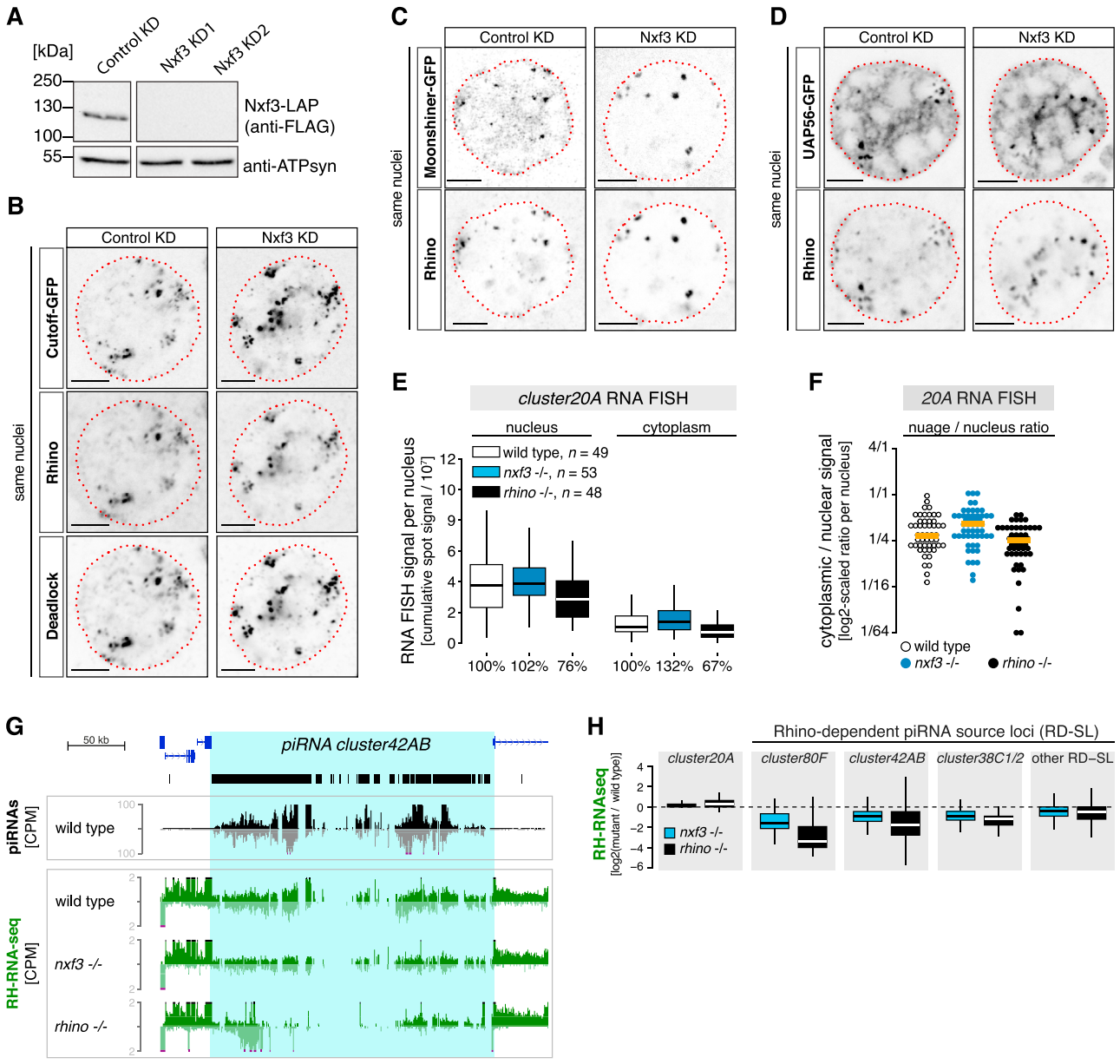

Figure S3. Related to Figure 2

(A) western blot verifying the efficiency of two independent sh-RNA lines against Nxf3. sh-RNA lines were expressed with MTD-Gal4 in ovaries expressing Nxf3-LAP. A staining against ATP-synthase serves as loading control.

(B-D) Confocal images (scale bar: 5 μm) confirming that loss of Nxf3 (depleted via sh-RNA expression) does not impact enrichment of Cutoff, Rhino, Deadlock (B), Moonshiner (C), or UAP56 (D) at nuclear Rhino foci (piRNA clusters). Red lines: nuclear envelope based on DAPI signal.

(E) Quantification of *cluster20A* RNA FISH signal in nurse cells with indicated genotype (boxplot definition as in Figure 2B; number of analyzed germline nuclei indicated).

(F) Ratio of total *cluster20A* RNA FISH signal in nuage and nucleus quantified per nurse cell nucleus (genotypes indicated; orange bars: median values).

(G) UCSC genome browser panel showing ovarian steady state RNA levels (CPM: coverage per million reads; total RNA-seq after depletion of rRNA) at *cluster42AB* in indicated genotypes.

(H) Boxplot displaying log2 fold changes in steady state RNA levels (RNA-seq) at indicated genomic loci in ovaries of indicated genotypes (respective to control samples). Contrasted is the Rhino-independent piRNA *cluster20A* against Rhino-dependent piRNA clusters (*42AB*, *80F*, *38C1+2*, others). Individual data points underlying the boxes are genomic 1-kb tiles, only reads mapping uniquely to each locus were considered. Boxplot definition as in Figure 2B.

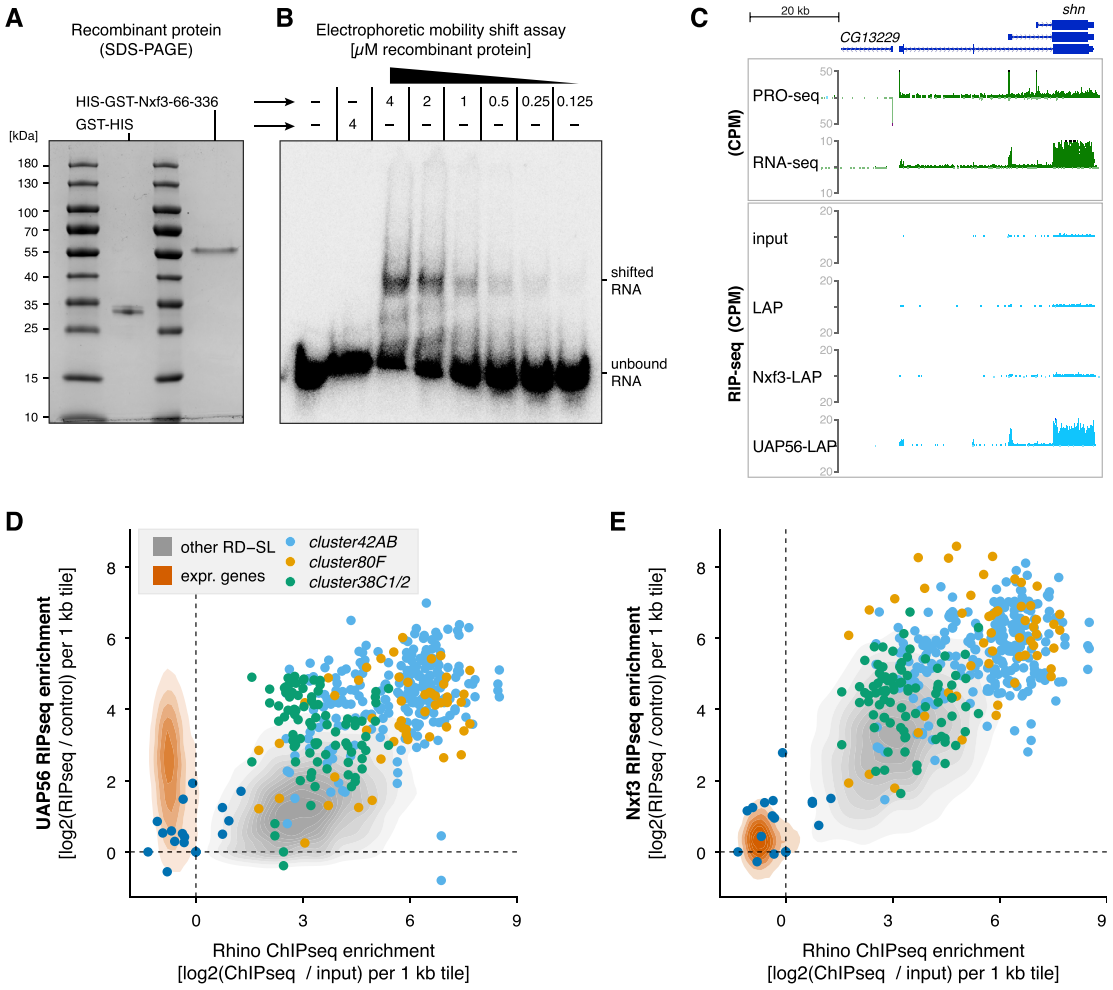

Figure S4. Related to Figure 3

(A) Coomassie stained PAGE gel showing purity of recombinant GST-tagged Nxf3 RNA binding domain (residues 66-336).

(B) Native PAGE gel displaying gel shift of a radioactively labeled single-stranded RNA oligo upon addition of different amounts of the recombinant Nxf3 RNA binding domain.

(C) UCSC genome browser panel showing transcriptional output (PRO-seq), steady state RNA levels (RNA-seq) and RIP-seq signal in ovaries of indicated genotype at the *schnurri* locus. CPM: coverage per million reads.

(D–E) Scatterplots showing RIP-seq enrichment for UAP56 (D) or Nxf3 (E) versus Rhino occupancy. Contrasted are genomic 1-kb tiles mapping to Rhino-dependent piRNA source loci (gray; major clusters shown as colored dots) versus genomic tiles overlapping expressed protein-coding genes (orange). Genomic 1-kb tiles belonging to the Rhino-independent piRNA *cluster20A* are shown in dark blue.

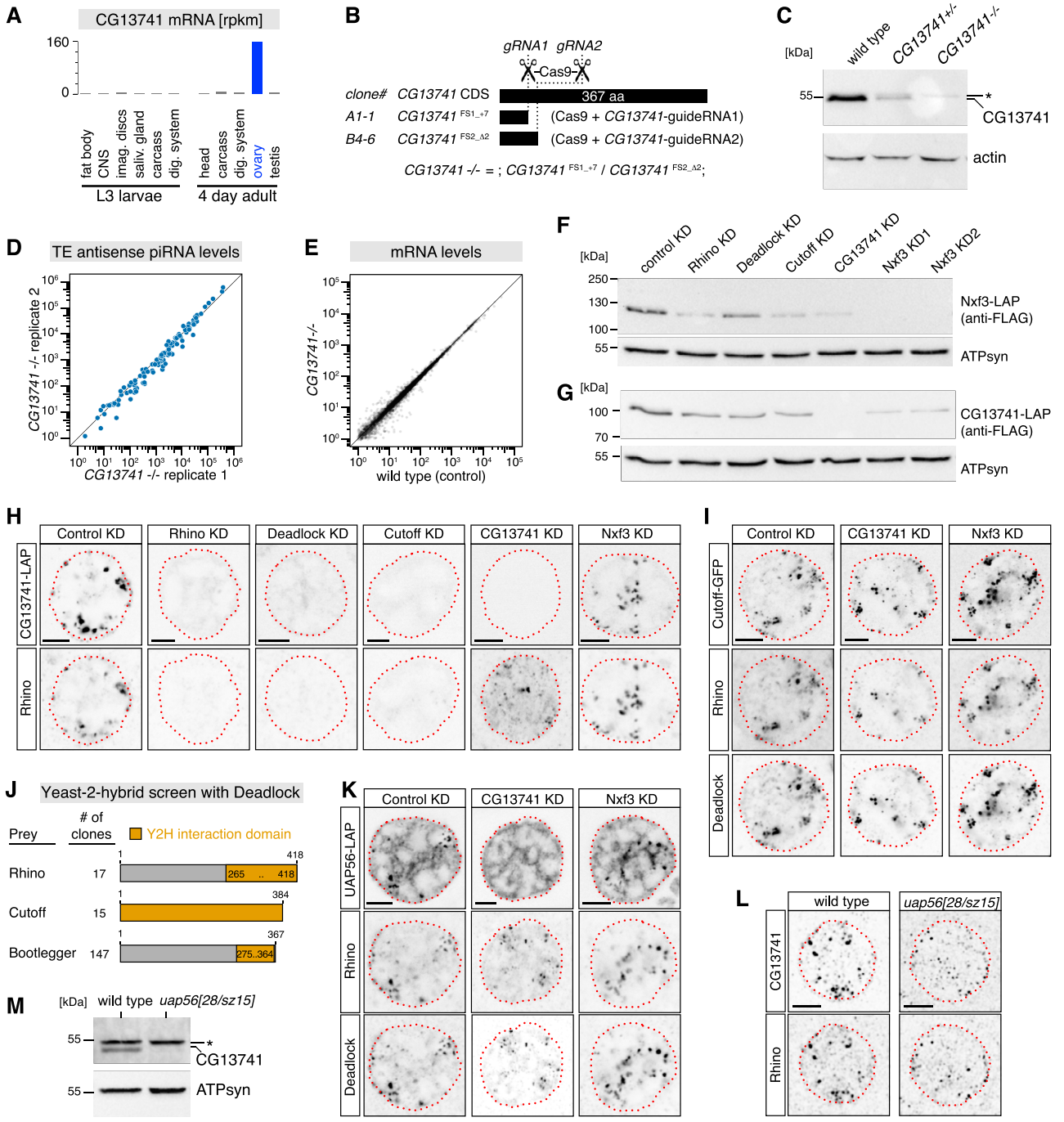

Figure S5. Related to Figure 4 and 5

(A) Shown are mRNA levels as determined by RNaseq for *CG13741* from indicated larval or adult tissues (data from Flybase (Brown et al., 2014)).

(B) Cartoon depicting the frameshift mutations in *CG13741* generated by CRISPR/Cas9 using two independent single guide RNAs. The allelic null allele combination used throughout this paper is indicated at the bottom.

(C) western blot analysis using a monoclonal antibody raised against CG13741 verifying the *CG13741* mutant frameshift alleles (the asterisk marks an unspecific band). A staining against actin served as loading control.

(D) Scatterplot displaying levels of antisense piRNAs mapping to consensus transposon sequences from the two replicate *CG13741* mutant samples.

(E) Scatterplot displaying steady state mRNA levels (transcripts per million sequenced transcripts) from ovarian samples of indicated genotype.

(F–G) western blots showing levels of endogenously tagged Nxf3-LAP (F) or CG13741-LAP (G) in lysates from ovaries of indicated genotype (KD: germline specific sh-RNA mediated knockdown). A staining against ATP-synthase served as loading control.

(legend continued on next page)

(H, I, K, and L) Confocal images of nurse cell nuclei (each column is the same nucleus; genotypes indicated at top) displaying localization of either CG13741-LAP and Rhino (H), Cutoff-GFP, Rhino, and Deadlock (I), UAP56-LAP, Rhino, and Deadlock (K), or CG13741-LAP and Rhino in a *uap56[28/sz15]* mutant nurse cell (L). Scale bars: 5 μm. Red dotted lines: based on DAPI (H, I, and K) signal or WGA (L).

(J) Cartoon depicting all prey clones retrieved from a yeast two-hybrid screen using full-length Deadlock as bait and employing a *Drosophila* ovarian cDNA library.

(M) western blot analysis showing CG13741 levels in control and *uap56[28/sz15]* ovary lysates (asterisk: unspecific band). A staining against ATP-synthase served as loading control.

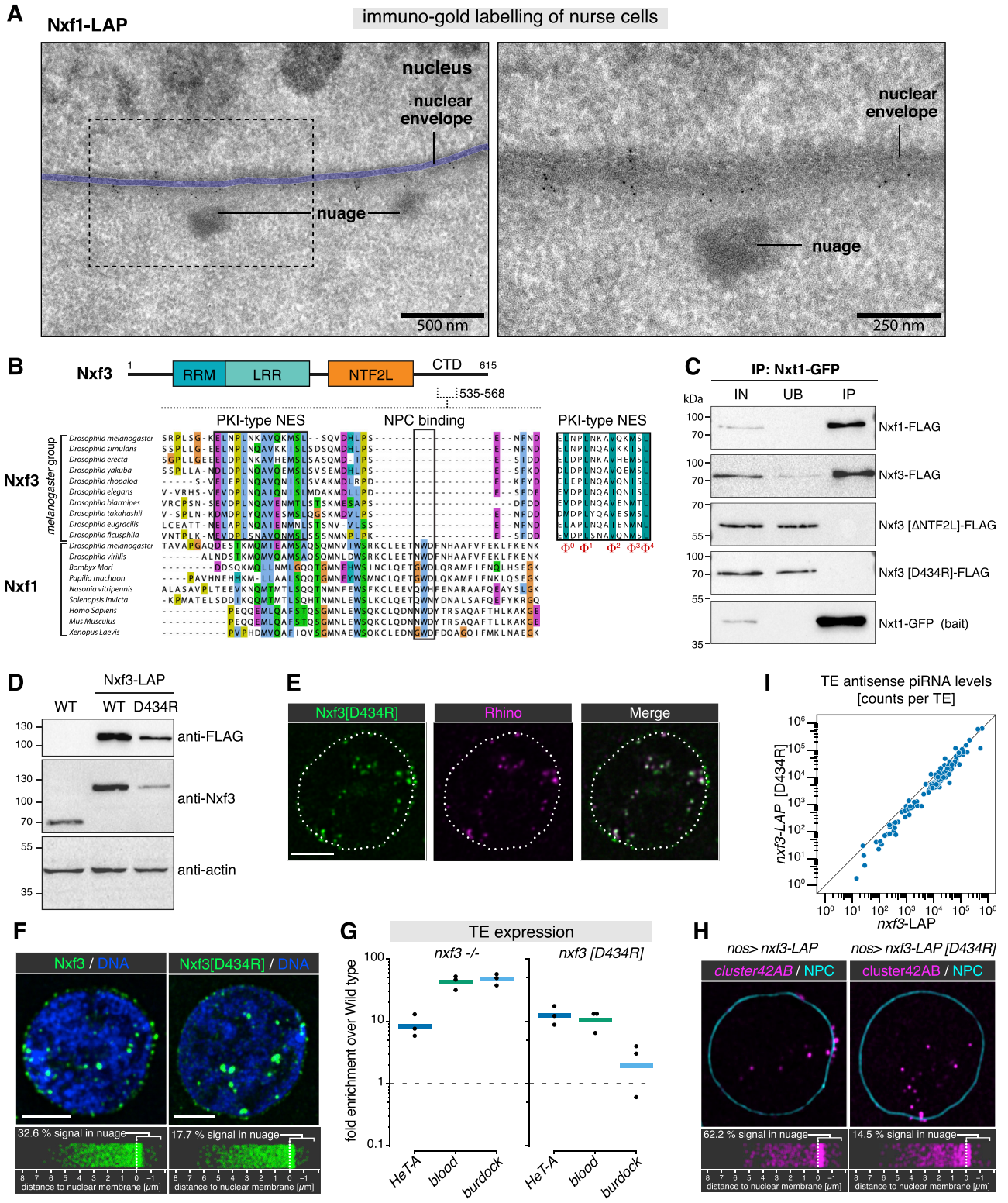

Figure S6. Related to Figure 6

(A) Transmission electron microscopy images of nurse cells expressing Nxf1-LAP at different magnifications. The nuclear envelope is pseudo-colored (blue), also indicated are nuage (electron-dense perinuclear structures), and nucleus. Sections were stained with a polyclonal anti-GFP antibody and a secondary anti-rabbit antibody coupled to 6nm gold particles.

(legend continued on next page)

(B) Protein sequence alignment displaying the nucleoporin interacting motif in Nxf1 proteins, as well as the position of the PKI-type NES motif in Nxf3 proteins. The NES core features (hydrophobic residues required for Crm1 interaction) are shown to the right.
(C) western blot analysis of Nxt1-GFP co-immuno-precipitation experiments where indicated FLAG-tagged Nxf1 or Nxf3 constructs were co-transfected in S2 cells.
(D) western blots indicating levels of endogenous Nxf3 (lane 1) and endogenously tagged Nxf3-LAP (lane 2: wild-type Nxf3-LAP; lane 3: Nxt1 interacting mutant Nxf3-LAP).
(E) Confocal images of a nurse cell nucleus (scale bar: 5 μm; white dotted line: nuclear envelope) showing co-localization of Nxf3-LAP [D434R] (green) and Rhino (magenta).
(F) Confocal images of representative nurse cell nuclei (scale bar: 5 μm) showing localization of indicted Nxf3-LAP proteins (DAPI: blue). Jitter plots below indicate the distance of Nxf3-LAP protein foci to the nuclear envelope (n = 1500 foci analyzed per genotype).
(G) Shown are changes in steady state RNA levels of indicated transposons (as determined via qRT-PCR) in ovaries of indicated genotype versus Wild-type control (n = 3; bar marks mean).
(H) As in (F), but instead of Nxf3 signal, *cluster42AB* FISH signal is shown (same nucleus as in (F) is shown).
(I) Scatterplot displaying levels of antisense piRNAs mapping to consensus transposon sequences from control ovary samples (CI: Nxf3-GFP endogenous knock-in) versus *nxf3[D434R]* mutant samples.

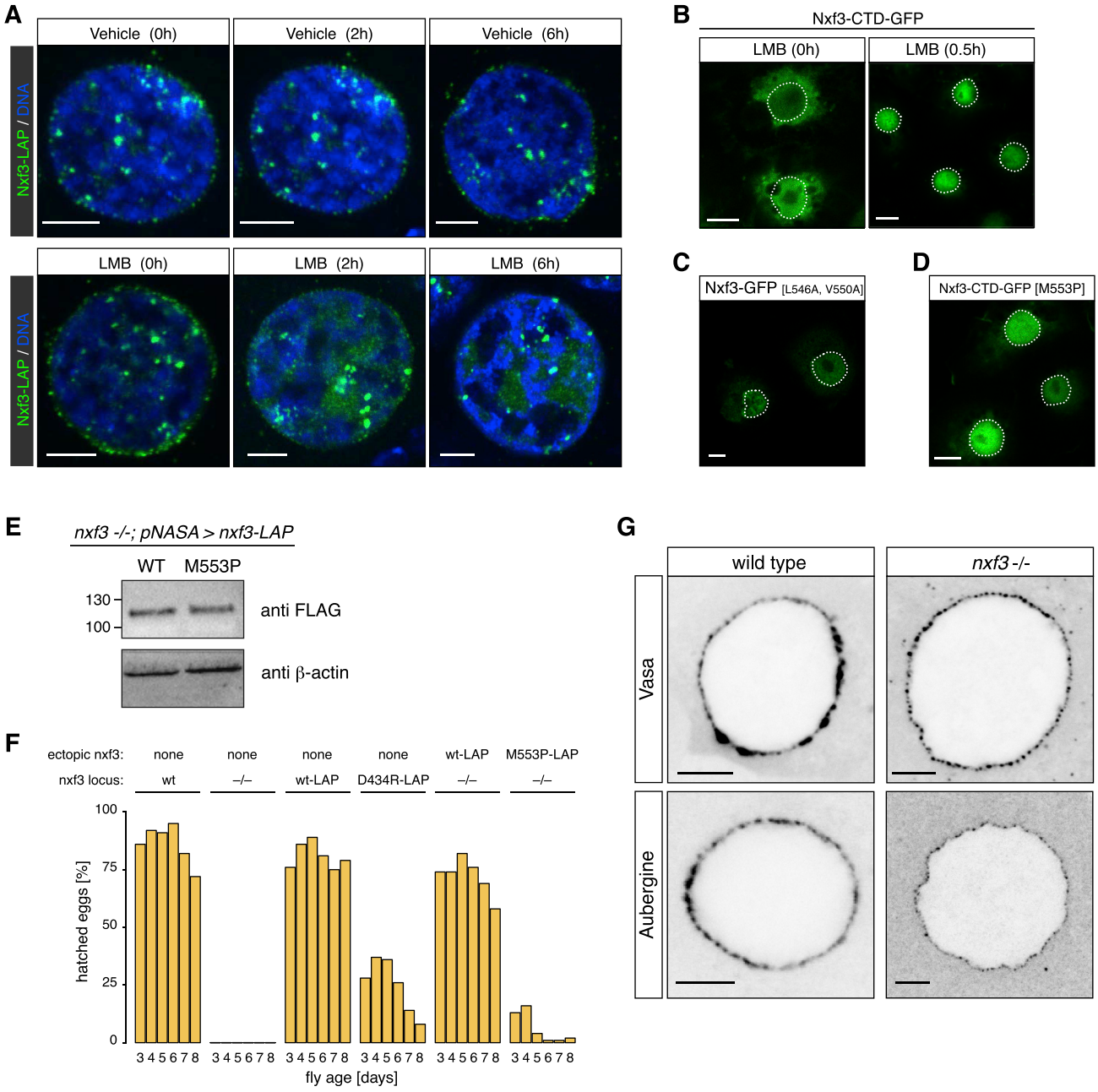

Figure S7. Related to Figure 6

(A) Confocal images showing sub-cellular localization of Nxf3-LAP in ovaries treated for indicated times with the Crm1 inhibitor LMB (bottom row) or carrier (70% methanol; top row; scale bar: 5 μm). Note the loss of Nxf3-LAP signal in nuage upon LMB treatment.

(C) Confocal image showing sub-cellular localization of Nxf3-GFP [L546A, V550A] in S2 cells (scale bar: 5 μm).

(B) Confocal images showing sub-cellular localization of Nxf3-CTD-GFP in S2 cells treated with the Crm1 inhibitor LMB (scale bar: 5 μm; dotted line marks nuclear envelope).

(C) Confocal image showing sub-cellular localization of Nxf3-GFP [L546A, V550A] in S2 cells (scale bar: 5 μm).

(D) Confocal image showing sub-cellular localization of Nxf3-CTD-GFP [M553P] in S2 cells (scale bar: 5 μm).

(E) western blot analysis showing levels of *nanos* promoter driven Nxf3-LAP (Wild-type versus NES mutant) in ovaries mutant for endogenous *nxf3*.

(F) Bar plot summarizing hatching rate (in percent) of eggs laid by females of indicated age and genotype mated to wild-type males.

(G) Confocal images of nurse cells (genotype indicated on top; scale bar: 5 μm) expressing Vasa-GFP or Aubergine-GFP. Nuage granules are smaller, but clearly present in ovaries mutant for *nxf3*.